Supramolecular arrangement of molybdenum carbonyl metallosurfactants with CO releasing properties

Elisabet Parera,[†,§] Maribel Marín-García,[†,‡] Ramon Pons,[‖] Francesc Comelles,[‖] Joan Suades*[,§] and Ramon Barnadas-Rodríguez*[,‡]

[‡]Unitat de Biofísica/Centre d'Estudis en Biofísica, Facultat de Medicina, Departament de Bioquímica i Biologia Molecular, Universitat Autònoma de Barcelona. 08193 Cerdanyola del Vallès, Catalonia, Spain.

[§]Departament de Química, Edifici C, Universitat Autònoma de Barcelona, 08193 Cerdanyola del Vallès, Catalonia, Spain

[‖]Institut de Química Avançada de Catalunya, IQAC-CSIC, Jordi Girona, 18-26, 08034 Barcelona, Catalonia, Spain.

[†] Both authors have contributed equally to this work.

Supporting Information

ABSTRACT: Two families of molybdenum carbonyl metallosurfactants, $Mo(CO)_5L$ and $Mo(CO)_4L_2$, were synthesized using the functionalized phosphines, $Ph_2P(CH_2)_nSO_3Na$ (n = 2, 6, 10) and characterized by the usual spectroscopic and spectrometric methods. The study of the supramolecular arrangements of these compounds in aqueous medium has been performed by surface tension, fluorescence, dynamic light scattering, cryo-TEM, and small angle X-ray scattering. All data points to the formation of medium and large vesicular structures with a membrane similar to the classical lipid bilayer, but it contains organometallic fragments instead of simple hydrophobic chains. Studies of CO releasing with these molybdenum carbonyl metallosurfactants have shown their viability as a promising CO releasing molecules.

INTRODUCTION

The term "metallosurfactant" was created in the 1990's, and it is commonly used to design molecules that behave as surfactants and contain a metal atom in the molecular structure.[1, 2] Since a simple design of a surfactant is commonly based on a molecule that has a linear hydrophobic chain and a polar headgroup, an important group of metallosurfactants are molecules in which the metal atom is the polar headgroup of the surfactant. A classic example of this kind of metallosurfactants is a metal complex of metals like Ni^{2+} or Cu^{2+} with an aliphatic amine that incorporates a long hydrophobic chain, as shown in Scheme 1.[1, 3] Although, in some reports, the term metallosurfactant has been associated with this design,[3] it is evident that other approaches are possible. Hence, an excellent example of an alternative design for metallosurfactants is found in metal complexes of functionalized phosphines, in which the phosphine contains a hydrophobic group and a polar group, such as sulphonate.[2, 4, 5] In this approach, the polar headgroup and the hydrophobic group are located in the molecular structure of the ligand, and consequently, the ligand can act as a surfactant independently of whether it is free or linked to a metal atom. These former groups of ligands (surfactant phosphines) have been relevant in organometallic chemistry, as one important property of surfactants is the self-aggregation and accumulation at the interfaces; properties that have incentivized the study of metallosurfactants in catalytic reactions.[4, 6] However, in recent years, a wide range of others attractive possibilities has emerged for metallosurfactants based on the possible control of the supramolecular arrangements of metallic compounds, and in the use of these complexes in biology and medicine. Some examples are templates for mesoporous materials,[7] metallomesogens,[8] optoelectronic devices,[9] ultrathin redox-active surfaces,[10] nanoparticles,[11] labeling phospholipids membranes,[12] antimicrobial compounds,[13] and magnetic resonance imaging.[14]

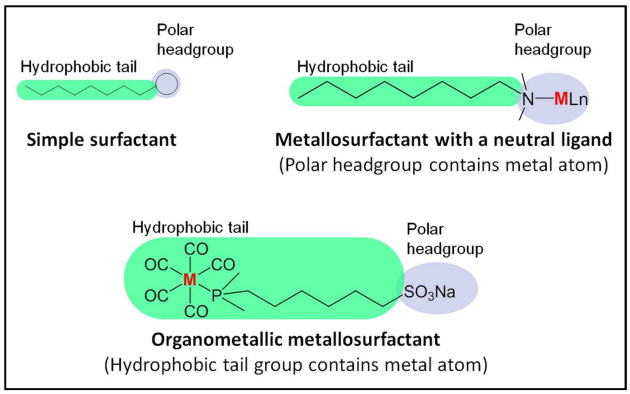

Scheme 1. Structures of different surfactants.

In a previous paper,[5] we reported the synthesis and study of a family of platinum metallosurfactants prepared from three surfactant phosphines **1-3** (Scheme 2). Both, free phosphines and cis-$PtCl_2L_2$ (L = **1, 2, 3**) complexes showed the characteristic aggregation properties of surfactants, and it was possible to study the influence of the hydrocarbon chain length in the aggregation properties of these metal complexes.

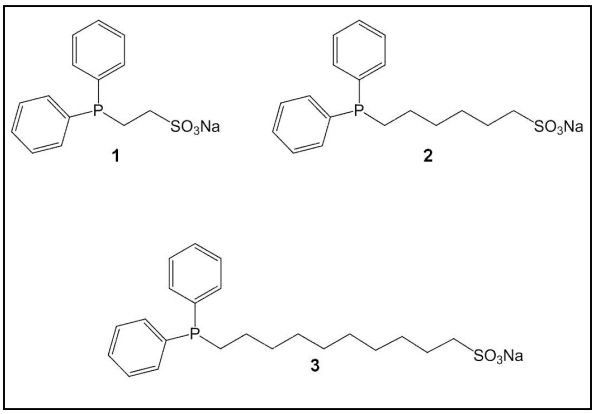

Scheme 2. Phosphine ligands 1-3.

In the present study, we have undertaken a novel approach that it is completely opposite to the design of the earliest metallosurfactants family (Scheme 1, metallosurfactant with neutral ligand). Thus, if in the first metallosurfactants, the metal is coincident with the polar head-group, in the current work the metal is included in the hydrophobic group (Scheme 1, organometallic surfactant). To attain this goal, the organometallic approach is very useful because it allows preparing metal fragments with the characteristic properties of organic hydrophobic groups. Very few examples of organometallic metallosurfactants have been reported, and most of them are based on ferrocene derivatives (ferrocenyl surfactants)[15] and, as far as we know, only one is based on metal carbonyls. However, this unique example is an alkoxy Re(I) complex that does not have an additional polar head-group, therefore it can be considered a metallosurfactant with the polarity located around the metal atom.[16]

Organometallic metallosurfactants based on metal carbonyls are attractive molecules because they can lead to singular supramolecular arrangements and, in addition, the presence of a metal carbonyl group makes it possible to use these compounds in different potential applications. As happens with conventional surfactants, which self-assemble in water, metallosurfactant molecules also form aggregated structures. In some cases they produce micelles, as classic surfactants do, but, in other cases they mainly generate vesicles, that is, membrane structures which enclose an aqueous compartment.[17] According to this scenario, a bilayer is the simplest packing arrangement of these molecules in the membrane (Scheme 3), like phospholipids do. As regards to the two different metallosurfactants shown in Scheme 1, bilayer arrangement implies two different locations for the metal atoms. In the first kind of metallosurfactant, the metal atoms should be located on the surface of the bilayer (Scheme 3, sketch A), whereas with the organometallic metallosurfactant the metal atoms have to be placed in the inner part of the bilayer (Scheme 3, sketch B), being part of its hydrophobic region. At this point, it is necessary to highlight that this approach allows placing organometallic fragments in structures that can mimic biomembranes, a design that is very attractive for possible uses of metals in medicine. In this context, we have focused this work in the potential applications of carbonyl metallosurfactants as CO releasing molecules (CORMs). More than ten years ago, Motterlini and co-workers showed the great potential of some metal carbonyls as therapeutic agents on the basis of the ability of these compounds for releasing CO in biological systems.[18] The therapeutic benefits of

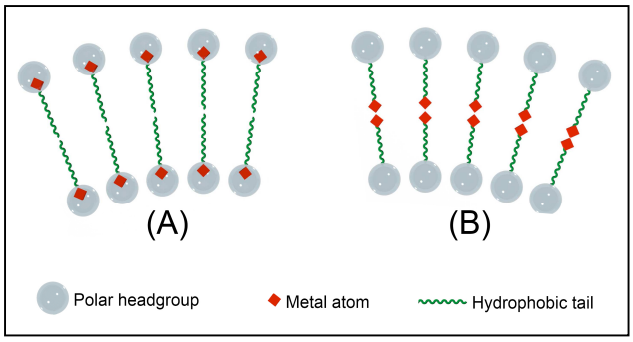

Scheme 3. Bilayer arrangement of metallosurfactants.

CORMs have been demonstrated in different studies, some examples are their anti-inflammatory and vasodilatory properties that make these compounds excellent candidates for the treatment of different diseases.[19] In spite of the large number of related publications reported, there is still a long way to go to achieve this goal, because it requires a control of dosage, timing and location of the CO. Hence, in this study we report on metal complexes that combine the ability to act as CO releasing molecules with the aggregation properties of metallosurfactants; therefore we can obtain supramolecular structures that can act as CO delivery systems. As far as we know, only one study has been reported that describes a micellar system that behaves as a CORM. However, due to the fact that it is based on polymeric micelles that contain a ruthenium carbonyl,[20] the previous approach is very different to that shown in the present paper.

Part of this work was previously communicated.[21]

RESULTS AND DISCUSSION

Synthesis and characterization of metallosurfactants

Molybdenum pentacarbonyl complexes **4-6** {[$Mo(CO)_5L$] (L = **1, 2, 3**)} were prepared from $Mo(CO)_6$ using methods similar to those reported for the related ionic complexes [$M(CO)_5$(TPPTS)] (TPPTS = sodium triphenylphosphine trisulfonate)[22] with some modifications in the experimental procedure (Scheme 4). Thus, complexes [$Mo(CO)_5L$] can be synthesized by direct reaction with $Mo(CO)_6$, or by a substitution reaction with a [$Mo(CO)_5L'$] complex that contains a labile L' ligand. We found that the direct reaction between $Mo(CO)_6$ and ligands **1-3** in a methanol/THF medium allows obtaining the complexes (**4-6**) using a convenient procedure and, in addition, it leads to pure products. This procedure is very useful to obtain small quantities (≈ 100 mg) of pure complexes **4-6**, but it has the problem that large quantities of $Mo(CO)_6$ are necessary to prepare the complexes on a larger

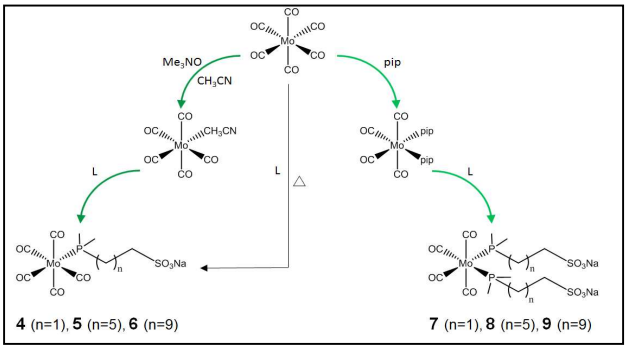

Scheme 4. Synthesis of molybdenum metallosurfacants 4-9 (pip = piperidine; L = ligand).

scale (≈ 1.0 g). To avoid this drawback, we have developed an alternative method based on the preparation of the reaction intermediate $[Mo(CO)_5(CH_3CN)]$ from $Mo(CO)_6$ by decarbonylation with Me_3NO and subsequent reaction with the phosphine (Scheme 4).[23] This method allows obtaining the desired products with similar purity levels, and it is not necessary to use a large excess of $Mo(CO)_6$.

Complexes **4**-**6** were characterized by usual spectroscopic (IR, ^1H, and ^{31}P NMR; see Supporting Information 1) and spectrometric methods[21] (MS/ESI(-), HRMS). The IR spectra in the carbonyl region shows the characteristic three bands for $[Mo(CO)_5L]$ complexes with a pattern and positions nearly identical to those reported for the related complexes $[Mo(CO)_5(PPh_3)]$[24] and $[Mo(CO)_5(TPPTS)]$.[22] The ^{31}P NMR spectra display a singlet around 27 ppm for the three complexes, showing the normal shift of this signal after coordination to the $\{Mo(CO)_5\}$ fragment with respect to the position of free ligands **1**-**3** (≈ -16 ppm). The ^1H NMR spectra agree with the proposed structure and, if we compare with the spectra of the free ligands, the shift of peaks assigned to methylene groups linked to phosphorus atom after coordination to the metal atom can be observed. Unfortunately, ^{13}C NMR spectra could not be obtained due to the low solubilities of complexes **4**-**6**.

The ESI-MS spectrometry (negative ionization mode) of **4**-**6** agree with the proposed stoichiometries, and it shows the signals of the respective anions [M-Na] and/or signals in which some carbon monoxide molecules have been eliminated as [M-2CO-Na]. We note that the loss of CO molecules decreases with the increase of the alkyl chain. Thus, using identical experimental conditions, with complex **6** the sole peak observed, corresponds to [M-Na]. In complex **5** the same signal is observed but also a peak that corresponds to [M-2CO-Na] and, finally, for complex **4**, the peaks that correspond to fragments as [M-2CO-Na], [M-3CO-Na] and [M-4CO-Na] can only be seen. The signals corresponding to the [M-Na] anions for the three complexes (**4**-**6**) could be observed in the HRMS-ESI-MS(-) spectra. It should be highlighted the great coincidence between the isotopic pattern of calculated and experimental spectra for the three complexes.[21]

The metal complexes **7**-**9** {$[Mo(CO)_4L_2]$ (L = **1**, **2**, **3**)} were prepared from the complex $[Mo(CO)_4(pip)_2]$, which contains two labile piperidine ligands (Scheme 4), following the reported method for other $[Mo(CO)_4L_2]$ (L= neutral phosphine) complexes,[25] but with some significant differences in the reaction medium due to the ionic nature of ligands **1**-**3**. Hence, **7**-**9** were synthesized using a synthetic method similar to that reported for $[Mo(CO)_4(TPPTS)_2]$,[26] but the experimental conditions had to be optimized in order to obtain pure products. Thus, the study of this reaction in an NMR tube (Figure 1) showed the formation of an intense signal at 31.4 ppm that has been assigned to the reaction intermediate $[Mo(CO)_4(pip)(\mathbf{1})]$. This assignment agrees with the fact that this signal is relevant in experiments at short reactions times, and also if the ratio between the precursor $[Mo(CO)_4(pip)_2]$ and the phosphine ligand is high. Taking into account these results, the posterior fine-tuning of the reaction conditions (reaction time, reagents ratio and solvents volumes) allowed the preparation of the *cis*-$[Mo(CO)_4L_2]$ (L = **1**, **2**, **3**) complexes with high yield (≈ 80 %) and purity.

Characterization of **7**-**9** using the spectroscopic methods (see Supporting Information 1 and reference 21) confirms the proposed *cis*-$[Mo(CO)_4L_2]$ structure for these complexes. The IR spectra show, in the carbonyl region, the characteristic four bands of complexes with C_{2v} symmetry in positions very similar to those reported for the homologous complexes with PPh_3[24] and TPPTS[25] ligands. The ^{31}P NMR spectra of **7**-**9** show the expected singlet for *cis*-$Mo(CO)_4P_2$ coordination set with a chemical shift very similar to those observed for complexes **4**-**6**, but with a very small high field shift (≈ 1 ppm, see Figure 2), a behavior that has also been reported for other $[Mo(CO)_5L]$ and *cis*-$[Mo(CO)_4L_2]$ (L = phosphine) complexes.[27] The ^1H NMR spectra show all expected signals and, similarly to the above complexes **4**-**6**, the shifts of methylene groups located closer to the phosphorous atom after coordination to the metal atom can be observed. The ^{13}C NMR spectra of complexes **7**-**9** could be obtained because of the higher solubility of these compounds in methanol in respect to **4**-**6**. The assignment of significant signals corresponding to the coordinated ligands has been performed by means of 2D ^1H, ^{13}C-HSQC experiments. It is worth noting the resonances of carbonyl groups, which are observed as two signals of different multiplicity at 215 and 210 ppm, and they are respectively assigned to the CO in *cis*,*cis*-position and *cis*-*trans*-position to the phosphorous atom.

The ESI-MS spectrometry (negative ionization mode) of **7**-**9** confirms the proposed stoichiometries showing the signals of the respective anions [M-Na] in all cases. Unlike results obtained for **4**-**6**, no significant peaks corresponding to CO elimination were observed. Finally, accurate mass measurements by HRMS-ESI-MS(-) spectrometry provided exact masses of the main peaks [M-Na] for **7**-**9**, which corresponds to the proposed molecular formulas.

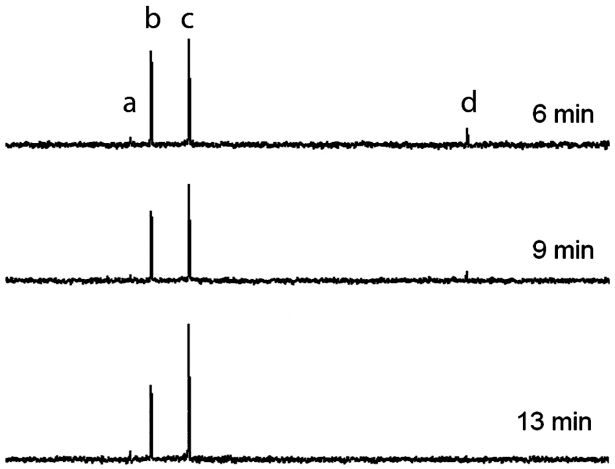

Figure 1. NMR spectra acquired during the reaction for the synthesis of **7** . a) $Ph_2P(O)(CH_2)_2SO_3Na$ at 34.5 ppm; b) intermediate at 31.4 ppm; c) *cis*-$[Mo(CO)_4(\mathbf{1})_2]$ at 25.7 ppm; d) $Ph_2P(CH_2)_2SO_3Na$ (**1**) at -15.7 ppm.

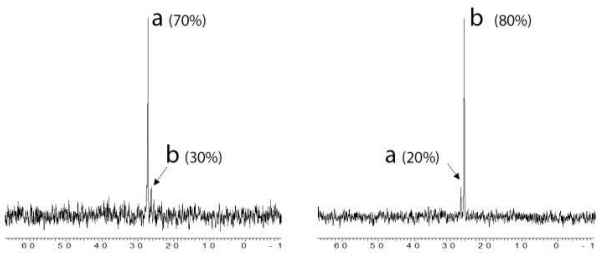

Figure 2. Comparison between the $^{31}P\{^1H\}$-NMR spectra of mixtures of complexes $[Mo(CO)_5(\mathbf{2})]$ (a) and cis-$[Mo(CO)_4(\mathbf{2})_2]$ (b) at different ratios.

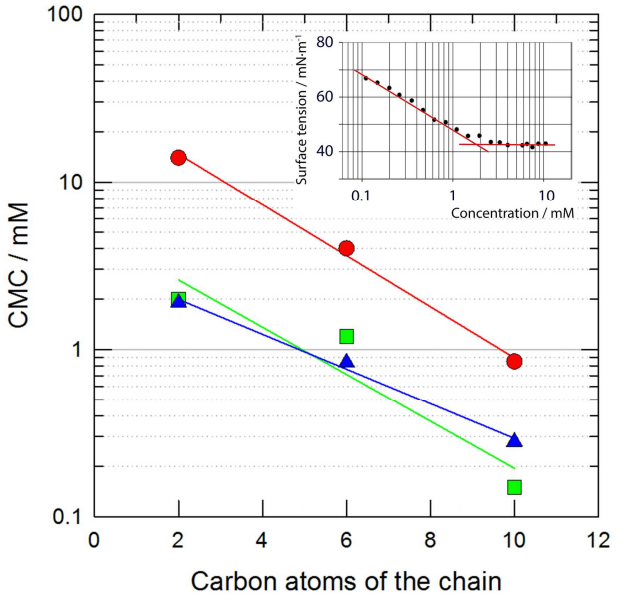

Figure 3. CMCs of ligand phosphines **1**, **2** and **3** (red circles), pentacarbonyl complexes **4**, **5** and **6** (green squares) and tetracarbonyl complexes **7**, **8** and **9** (blue triangles), as function of the carbon atoms of each hydrocarbon chains. Inset: Surface tension measurement of **7** as function of the concentration.

Attempts to prepare *trans*-$[Mo(CO)_4L_2]$ (L = **1**, **2**, **3**) complexes by isomerization of *cis*-$[Mo(CO)_4L_2]$ were unsuccessful. Although it is well-known that the more thermodynamically stable isomer *trans*-$[Mo(CO)_4(PPh_3)_2]$ complex can be prepared by simply heating a solution of *cis*-$[Mo(CO)_4(PPh_3)_2]$, the study of this reaction with **7**-**9** in non-polar solvents showed that the starting products are recovered even using long reaction times. This behavior can be associated with the low solubility of **7**-**9** in non-polar solvents. On the other hand, the ^{31}P NMR study of this reaction in more polar solvents as mixtures of THF/MeOH has demonstrated that the thermal decomposition of *cis*-$[Mo(CO)_4L_2]$ compounds leads to the formation of mixtures of the initial complex and the respective $[Mo(CO)_5L]$ compound. A similar behavior has been reported for the *cis*-$[Mo(CO)_4(TPPTS)_2]$ complex.[26]

Aggregation studies by surface tension and fluorescence measurements

Plots of surface tension versus concentration for the aqueous solutions of **1**-**9**[21] show a break point, that is, a change in the slope of the curve, which is characteristic of the formation of aggregates (Inset Figure 3). It is known that, below this point (critical micelle concentration, CMC), almost all amphiphiles are in the monomeric form, although in some cases the formation of dimers or oligomers has been reported,[28] or even predicted by molecular dynamics.[29] At surfactant concentrations higher than the CMC, they undergo self-aggregation and produce, for example, micelles or vesicles. Figure 3 shows the CMC obtained for the different surfactants studied in the present work. As can be observed, it reveals that the evolution of the critical concentrations depends both on the type of molecule (that is, phosphine ligands **1**-**3**, pentacarbonyl **4**-**6** and tetracarbonyl **7**-**9** complexes) and on the total number of carbon atoms of their hydrocarbon chains. The first dependence can be explained by the different composition of the hydrophobic end of each type of molecule. The coordination of the surfactant phosphine ligands with a rigid non-polar group, such as $\{Mo(CO)_4\}$ or $\{Mo(CO)_5\}$, produces a significant

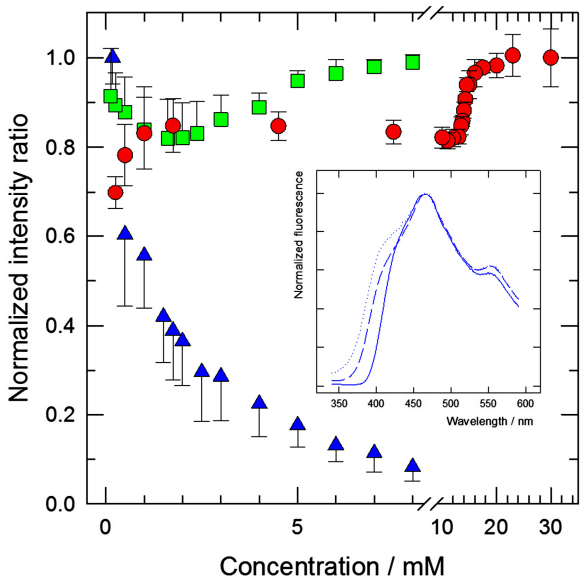

Figure 4. Normalized fluorescence intensity ratios of **1** (red circles; I396 nm/I464 nm, excit. 250 nm; n= 6); **4** (green squares; I566 nm/I466 nm, excit. 305 nm; n= 4); and **7** (blue triangles; I396 nm/I467 nm, excit. 305 nm; n= 4). Results: mean ± standard deviation. Inset: Normalized fluorescence spectra (excitation at 305 nm) of **7** in water at 8 mM (continuous line), 1.75 mM (dashed line) and 1 mM (dotted line).

decrease in the CMC. The second dependence is a well-known phenomenon. It is explained by the increase in the hydrophobic attraction between the surfactants with increasing the hydrophobic chain length. On the other hand, the changes in the shape and intensity of the fluorescent spectra of the **1**, **4**, **7** family obtained at different concentrations indicate that this technique is also useful for the determination of the CMC of these compounds. The inset of the Figure 4 shows several normalized spectra for the case of metal complex **7**. The evolution of the described variation was characterized by obtaining the intensity ratio at two emission wavelengths, corresponding to local maxima or to significant shoulders. The representation of these values versus the concentration al-

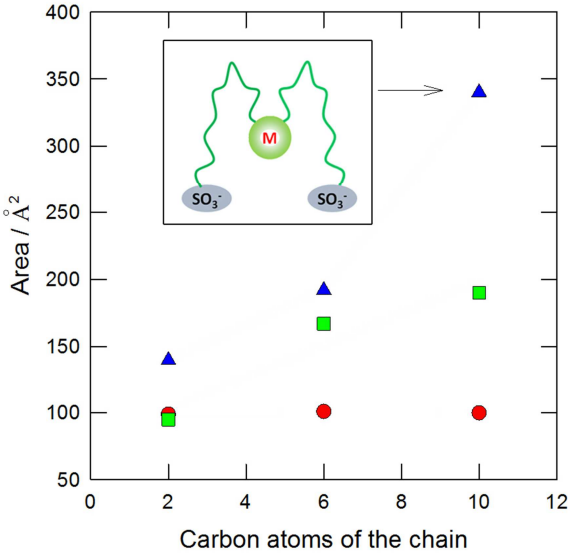

Figure 5. Estimated area occupied per molecule adsorbed in the water/air interface obtained from the surface tension measurements of water solutions of the compounds **1**-**3** (red circles), **4**-**6** (green squares), and **7**-**9** (blue triangles). Inset: Scheme of the double loop conformation of **9**.

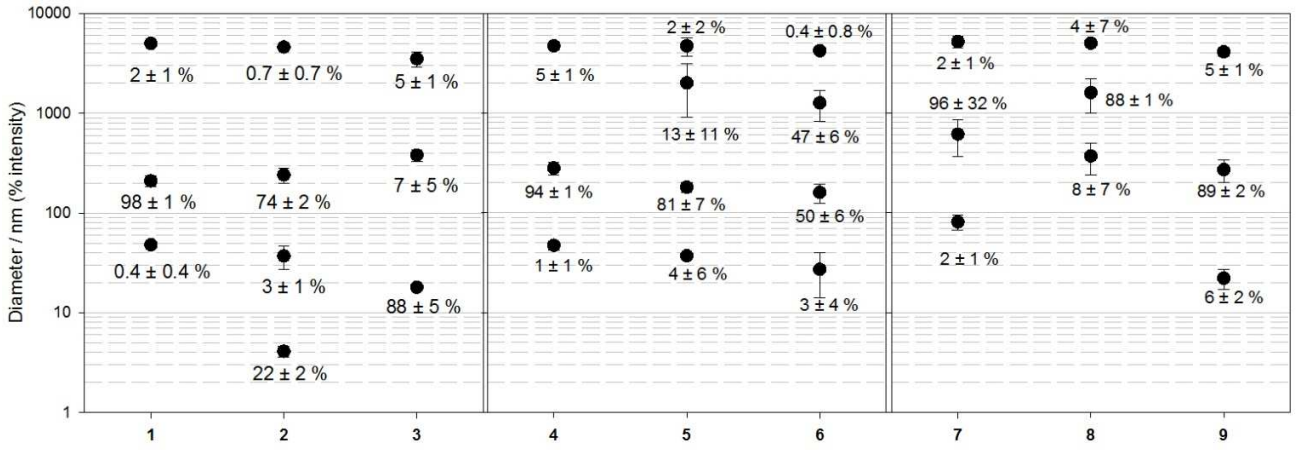

Figure 6. Size distributions of the aggregates formed by the phosphine ligands (**1**-**3**), pentacarbonyl (**4**-**6**) and tetracarbonyl (**7**-**9**) surfactants. The numbers adjacent to the points indicate the relative amount of each population. For each type of molecule (ligand, pentacarbonyl, and tetracarbonyl) the mean diameter of the sub-populations are shown in the common left axis, and their relative amount are expressed as percentage beside the corresponding symbol. Results: mean ± standard deviation.

lowed detecting breakpoints in the curves (Figure 4). The calculated values were 2 mM for **4** and **7**, and 14.2 mM for **1**. These concentrations are equivalent to that obtained by surface tension measurements. In the case of ligand **1**, a second breakpoint (not detected by surface tension measurements) was detected at, approximately, 1.5 mM. This fact could be caused by the formation of pre-vesicular aggregates, a phenomenon described in other charged surfactants.[28] Thus, from the surface tension and fluorescence measurements, it is clear that all the molybdenum carbonyl complexes undergo self-aggregation processes in aqueous media.

In addition, the surface tension data allowed obtaining the surface excess concentration (Γ) and the estimated area per molecule (A) in the air/water interphase. Although the absolute values obtained by this technique were questioned by some authors,[30] their relative values make it possible to compare the characteristics of a family of similar molecules. As can be seen in Figure 5 (and Supporting Information 2), the free phosphines **1**-**3** display no relevant differences between the values of A and, consequently, packing should be very similar with the sulphonate group in water and the lipophilic $(CH_2)_n$-PPh_2 group in an extended chain conformation. This is not the case for the pentacarbonyl **4**-**6** and tetracarbonyl **7**-**9** complexes, a result that can be attributed to the existence of the voluminous hydrophobic metal carbonyl group. In these molecules, the increment of the chain length of the complexes causes a progressive decrease in the molecular packing. This effect agrees with an increment of the cross-sectional area of the hydrophobic part of the molecules, a phenomenon well-described by the packing parameter,[31] which, for example, in the case of lipids, is modulated by the free rotation of the carbon-carbon bonds of their hydrocarbon chains. Note that there is a great increment in the area per molecule from **8** to **9**, not observed in the other cases. This result parallels the behavior previously observed with cis-$[PtCl_2L_2]$ (L = 1, 2, 3) complexes[10] and is consistent with a double loop conformation of the complex in the interface (Figure 5 and Supporting Information 2).[21]

Size analysis

The surfactant water solutions obtained did not pellet after their centrifugation, which indicates that aggregates were well formed. To analyze the size of the aggregates, aqueous solutions of **1**-**9** were studied by dynamic light scattering spectroscopy (DLS). All the experiments were carried out above the CMC of the molecules and, therefore, the results correspond to the supramolecular aggregates formed by the metallosurfactants. The mean hydrodynamic diameter and the polydispersity index (PDI) of the studied solutions are shown in Table 1. The mean diameters have a small error, which indicates not the width of the population, but the reproducibility of the analyses. The theoretical values for PDI range from 0 (absolutely monomodal distribution) to 1 (multimodal distribution) and, consequently, the experimental values obtained show that the spontaneously formed aggregates form polydisperse populations. This is a common phenomenon, taking into account that the suspensions were prepared by vortex, that is, no size control, such as, for example, extrusion, was performed. The size distributions plotted in Figure 6 clearly show this circumstance, as they show the existence of various sub-populations for each compound. In general, and due to their size, most of the populations are compatible with the existence of vesicular aggregates with entrapped water, which could be surrounded by one or more membranes of surfactant. In order to assign intervals, large (<1000 nm), medium (from 100 to 1000 nm), and small vesicles (from 20 to 100 nm), can be considered. As the size of the large aggregates are very close to the upper limit of detection of the instrument (about 6000 nm), the existence of a certain quantity of out of range vesicles should not be ruled out.

Compound	Concetration (mg/mL)	Mean diameter (nm; % intensity)	PDI
1	40.5	150 ± 20	0.44 ± 0.03
2	40.5	30 ± 4	1.00 ± 0.04
3	30.4	16 ± 1	0.30 ± 0.02
4	6.0	225 ± 4	0.41 ± 0.05
5	4.26	147 ± 2	0.46 ± 0.02
6	2.26	200 ± 20	0.70 ± 0.20
7	8.82	250 ± 80	0.56 ± 0.06
8	8.67	1300 ± 90	0.34 ± 0.05
9	4.00	127 ± 1	0.50 ± 0.01

Table 1. Particle size analysis of the substances **1**-**9**.

Morphology and structure of the aggregates

The physical characteristics of the spontaneously formed aggregates constituted by the surfactants in water were studied by Cryo-TEM and Small Angle X-ray Scattering (SAXS).

Cryo-TEM results agree with the DLS analyses, and in all cases the images (Figure 7) show the existence of medium and large vesicular structures. As regards the morphology, a huge quantity of multilayered vesicles was expected, because of the method of preparation (vortex). Surprisingly, this was not the case, since, as can be observed, the vesicles were constituted mainly by one or a few membranes, and in some cases multivesicular vesicles could be detected (but only with a few internal vesicles). Both phenomena (presence of medium size and monolayered vesicles) can be explained by the intense electrostatic repulsion between the membranes originating from the sulfonate groups of the surfactants. This influence of the charge on the size and lamerallity of the vesicles was also described in liposomes constituted by charged phospholipids.[32]

It is known that SAXS technique allows getting detailed information of the morphology of aggregates, as well as of their packing structure. For this reason, and with the aim of obtaining preliminary, and at the same time, representative results, the compounds **1**, **4** and **7** were studied by SAXS. Since they correspond to one of the three families synthesized, the results would monitor the effects caused by the structural differences among the molecules, that is, from one ligand to the corresponding complexes containing one or two hydrocarbon chains. In Figure 8, we show the experimental scattering curves for the ligand and both complexes and their corresponding best fits to the model, which corresponds to the lamellar arrangement present in vesicles, as is schematically shown in Scheme 3. Other models were also studied, and we found that the fitting of spherical models (micelles), although feasible, did not result in good absolute intensity scaling, or led to completely unphysical parameters. The parameters of the fits shown in Figure 8 correspond to the set of parameters shown in Table 2 and Supporting Information 3.

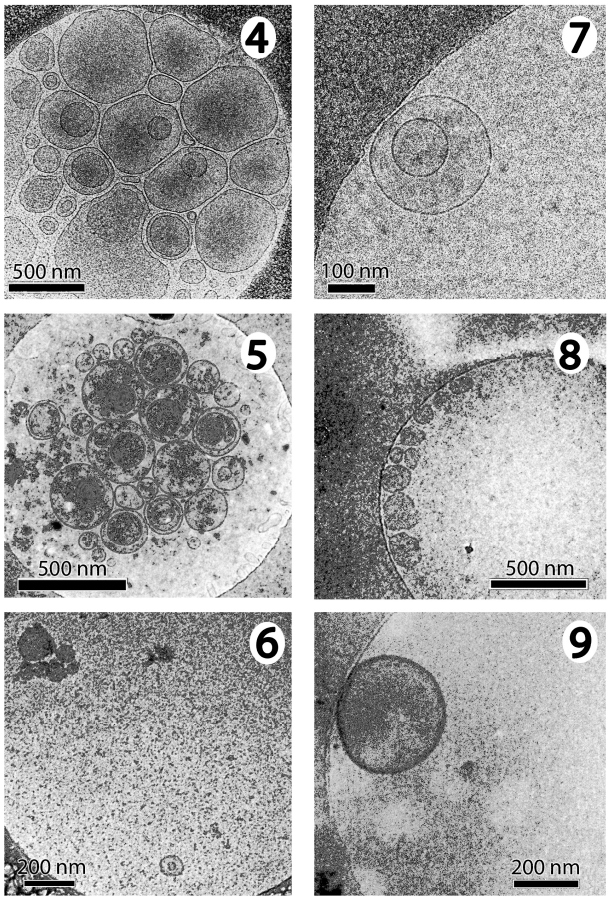

Figure 7. Cryo-TEM images of pentacarbonyl (**4**, **5** and **6**) and tetracarbonyl (**7**, **8** and **9**) complexes. The big light areas correspond to the holes of the grid, they are not vesicles.

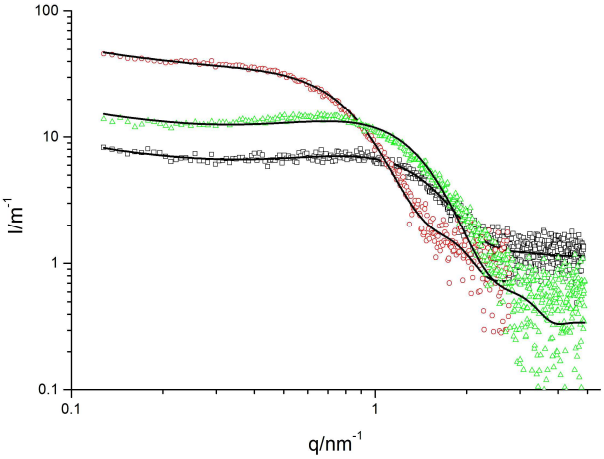

Figure 8. SAXS intensities as a function of scattering vector modulus (q) for dispersions of **1** (black squares), **4** (green triangles) and **7** (red circles).

The trend of the area per molecule (A_m) seems to have some logic. The ligand alone has an area per molecule that increases somewhat when the complex is formed, and the complex with two polar heads has an area per molecule comparable to the summation of the area per molecule of the pentacarbonyl complex plus an additional ligand. Those values can be compared with those obtained from surface tension results (Figure 5).

When comparing areas per molecule obtained from surface tension or other methods, we should bear in mind some of the problems associated with the application of Gibbs isotherm to surface tension,[33] as well as to the different situation corresponding to adsorption to the aqueous surface and to the formation of condensed phases. Apart from the problems associated with the sensitivity of surface tension to impurities (both hydrophobic and to multivalent counter-ions), the number of adsorbed species and the lack of direct relationship of surface saturation with micellation may produce discrepancies between the minimum area per molecule determined by surface

	1	**4**	**7**
A_m (Å^2)	49±3	72±6	153±10
L_c (nm)	0.74±0.02	1.13±0.02	0.75±0.02
L_h (nm)	2.25±0.05	4.22±0.2	2.48±0.05
V_c (nm^3)	0.363±0.025	0.814±0.070	1.15±0.080
V_h (nm^3)	1.10±0.07	3.04±0.29	3.79±0.26
N_w	34±5	100±10	115±10

Table 2. Molecular parameters of the surfactants when forming macromolecular aggregates obtained from the fitted curves shown in Figure 8.

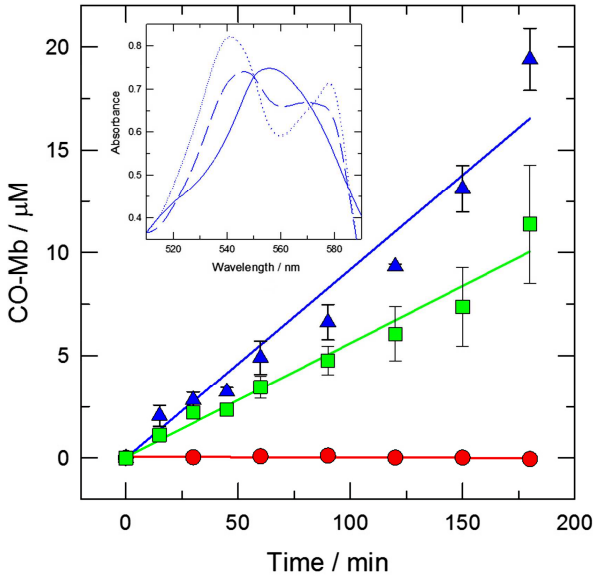

Figure 9. Kinetic of formation of CO-Mb in presence of **1** (red circles, negative control; n=2), **4** (green squares; n=3) and **7** (blue triangles; n=4) at 37ºC. Results: mean ± standard deviation. Inset: Reference spectra of deoxy-Mb (continuous line) and CO-Mb (dotted line), and that obtained as a consequence of the CO release from **7** (discontinuous line).

tension and the real minimum achievable area per molecule. This could be the case of ligand **1**, for which the surface tension and SAXS differ significantly. Part of the discrepancy could be attributed to the different situation corresponding to the adsorption to the interface and to the formation of a condensed phase, which is more restrictive in the sense that the molecules have to completely fill the space.[33] The hydrophobic volume (V_c) results from the product of the hydrophobic length (L_c) times A_m. It is apparent that the hydrophobic volume of the ligand plus that of the pentacarbonyl complex **4** is very close to that of the tetracarbonyl complex **7**. The hydrophobic length of the complex **7** is commensurate with the physical dimensions of the molecule, as obtained from ChemDraw (0.9 nm from the sulphonate methylene to the oxygen of the carbonyl plus the van der Waals radii of oxygen and half C-S bond), while that of complex **4** is slightly larger than that obtained from the ChemDraw configuration (1.0 nm from the sulphonate methylene to one of the protons of a benzene ring). The volume of the ligand, as obtained from a solvent excluded volume model (see Supporting Information 4), closely fits the experimentally fitted value, that is, 0.403 nm^3 from the excluded solvent model and 0.430 nm^3 for the summation of the experimentally fitted volume for the hydrophobic contribution (0.363 nm^3) plus the headgroup volume contribution (volume of the sulfonate group, 0.040 nm^3, and volume of the methylene group, 0.027 nm^3).[34] Giving this value for settled, we can estimate the contribution of the pentacarbonyl group as 0.451 nm^3, and that of the tetracarbonyl as 0.432 nm^3. Without additional reference, we can compare these values with the group volume, as also obtained from the solvent excluded volume. The results were 0.203 nm^3 for the pentacoordinated molybdenum and 0.185 nm^3 for the tetracoordinated molybdenum. Note that our experimental results gave values higher than the excluded solvent volumes. Our conclusion is that, because of the rigidity and bulkiness of the complexes, the packing in the hydrophobic part of the membrane is far from being compact. Considering the hydrophilic domain of the lamellae, the fitted length is considerably larger than the geometrical length of the polar groups. This matches with the high number of water molecules contained in the polar head, and calculated from the total polar volume minus the volume of the sulfonate group and methylene group. This also may be an indication of the large rugosity of this surface which is concomitant with the difficulties of packing of their bulky and rigid hydrophobic groups on a flat and compact layer

CO release tests

In order to check if the obtained molecules could be useful as CORMs, the ability of the ligand **1** (as control) and the metal carbonyl metallosurfactants **4** and **7** to release CO was evaluated according to the myoglobin assay (thus, as for the case of the SAXS study, the CO release was performed for the compounds of one family). It is based on monitoring, by UV-Vis spectroscopy, the conversion of deoxymyoglobin (deoxy-Mb) to carboxymyoglobin (CO-Mb) as a result of the release of the carbon monoxide from the metal complex. Thus, after incubating the indicated metal complexes with deoxy-Mb using previously reported experimental conditions, a clear increase of the peak corresponding to the CO-Mb complex with time was detected (Inset Figure 9), indicating that a release of CO from the metallosurfactants was produced. From these data, the time-evolution of the CO-Mb formation was plotted for metal complexes **4**, **7** (Figure 9). The phosphine ligand **1**, which has no CO group, was selected as a negative control. It did not cause any change in the spectrum of Mb, showing that the concentration of deoxy-Mb was maintained constant. In contrast, metal complexes **4** and **7** caused a continuous increase of the CO-Mb form, with initial rates of CO release $2.2 \cdot 10^{-4}$ mol CO·mol $CORM^{-1} \cdot min^{-1}$ (r^2= 0.9517) and $3.7 \cdot 10^{-4}$ mol CO·mol $CORM^{-1} \cdot min^{-1}$ (r^2=0.9631) for **4** and **7**, respectively. As can be observed, both molecules are characterized by a slow release of CO, and their corresponding half-lives were, 2250 min for **4** and 1360 min for **7**. The existence of CORMs with elevated half-life is a desired circumstance, as this behavior allows a sustained release of CO in the human body.[35] Thus, this preliminary study has shown that two preferred properties of CORMS converge in the studied metal complexes: They are water soluble molecules that self-assemble to form vesicles and they show high half-life for CO release. Consequently, they can be useful as therapeutic CO releasing vesicles.

CONCLUSIONS

Molybdenum carbonyl complexes with the surfactant phosphine ligands **1**-**3** have been synthesized and characterized by IR, NMR (^{1}H, ^{13}C, ^{31}P) and MS methods. All these metal complexes are water soluble and surface tension studies of these solutions have shown that they behave as surfactants, forming supramolecular aggregates at concentrations above the CMC. The size of these self-assembled structures was studied by DLS, which revealed the formation of various subpopulations of aggregates for each compound, in agreement with the formation of vesicular aggregates with entrapped water. This hypothesis was confirmed by cryo-TEM studies that show the presence of medium and large vesicles that contain predominantly one or a few membranes. This behavior can be related to an important electrostatic repulsion between the sulfonated groups located in the membrane surface. The

SAXS study of complexes **4** and **7** is concordant with DLS and cryo-TEM results, showing that the best fit with the experimental data is reached when a lamellar model is used, consistent with the formation of vesicular aggregates. This technique also suggests that the packing of the hydrophobic part, which contains the organometallic fragment, is less compact than it is in the conventional surfactants, an interesting result that should be confirmed in subsequent studies.

Finally, the CO releasing tests performed with the molybdenum carbonyl complexes **4**, **7** using the myoglobin assay have shown that these compounds exhibit a slow release of CO. These properties, in conjunction with their ability to form supramolecular structures at concentrations higher than their CMCs, make these metal complexes potential CORMs for therapeutic applications with no precedents in the literature.

EXPERIMENTAL SECTION

Synthetic and Characterization Methods.
All reactions were performed under nitrogen using standard Schlenk tube techniques. Tetrahydrofuran and methanol were distilled (respectively, over sodium/benzophenone and magnesium) and stored over 3Å molecular sieve. Pentane was dried with 3Å molecular sieve. Infrared spectra were recorded with a Perkin-Elmer 2000 FT spectrometer. The NMR spectra were recorded in the *Servei de Ressonància Magnètica Nuclear de la Universitat Autònoma de Barcelona* on Bruker DPX-250, DPX-360 and AV400 instruments. Microanalyses were performed by the *Servei d'Anàlisi Química del Departament de Química de la Universitat Autònoma de Barcelona (SAQ-UAB)*. Mass spectra and exact mass measurements were respectively obtained on an Esquire 3000 with electrospray ionization and an ion trap Bruker Daltonics and on a Bruker microTOFQ with electrospray ionization Apollo of Bruker by *SAQ-UAB*.

Ligands **1**-**3** were prepared using previously reported methods[5] and complexes **4**-**9** were synthesized and characterized following procedures reported in previous communication.[21] However, as discussed in the Result and Discussion section, a new more convenient method for preparing large quantities of complexes **4**-**6** has been recently developed, which is reported below.

Synthesis of Complexes 4-5
Trimethylamine N-oxide dihydrate (3.45 mmol) and molybdenum hexacarbonyl (4.14 mmol) were added to 15 mL of a dry dichloromethane-acetonitrile mixture (1:1), the resulting solution was protected from light and maintained under vigorous stirring at room temperature for 1.5 h. Next, a solution of the phosphine $Ph_2P(CH_2)_nSO_3Na$ (3.12 mmol) in dry methanol (30-40 mL) was slowly added and the mixture was allowed to stir at room temperature for additional 1.5 h. After this time, a yellow turbid solution was obtained, which was filtered through Celite to yield a clear solution. This solution was evaporated under reduced pressure to dryness and a yellow oil was obtained, which became a powdery yellow solid after scratching the walls with a spatula. This crude product was purified by dissolution in dry methanol (15-20 mL) and dropwise addition of freshly distilled diethylether (≈ 10 mL) until a thin white precipitate of $[Mo(CO)_6]$ was formed. The resulting mixture was centrifuged (10000 rpm) to eliminate the white solid and the filtrate was evaporated under reduced pressure to dryness in order to obtain the desired compound. Complexes **4**-**5** (1.490g for **4** and 1.527g for **5**) were isolated as brown solids. The ^{1}H-NMR, ^{31}P{1H}-NMR and IR spectra were consistent with previously reported data.

Particle size distribution
The size distributions of the aggregates formed by the ligands and metallosufactants were measured by dynamic light scattering (DLS) spectrometry using an UPA 150 (Microtrac Inc. FL. USA) and a Malvern Zetasizer ZS90 (Malvern Instruments Ltd., UK) particle analyzer. The instrument can detect particles which diameter ranges from 2 nm to 6 μm. Each data acquisition was a mean of 10 consecutive analyses, performed at 25ºC, without dilution of the sample (in order to not alter the phase equilibrium), and each experiment was repeated three times. To obtain the amphiphile solutions, previously recrystalized and lyophilized surfactants were resuspended and vortexed with degassed Milli-Q water. Solutions were allowed to equilibrate for 1 h previously to the analyses. Afterwards, samples were centrifuged in Eppendorf tubes (2-3 min, 13,000 rpm) to prevent the existence of any non-solubilized solid particle, which would interfere the analyses. Results are expressed as mean hydrodynamic diameter (% of intensity), main peaks of the sub-populations, and polydispersity index (PDI) with their corresponding standard deviations.

Cryo-Transmission Electron Microscopy
The morphology of the aggregates formed by the surfactants was studied imaging the suspensions by Cryo-electron microscopy (Cryo-TEM) at the *Servei de Microscòpia Electrònica de la Universitat Autònoma de Barcelona*. 2 μL of the aqueous samples were blotted onto holey carbon grids (Quantifoil) previously glow discharged in a BAL-TECMSC 010 glow discharger unit. They were subsequently plugged into liquid ethane at -180 °C using a Leica EM CPC cryoworkstation and observed in a Jeol JEM-1400 electron microscope operating at 120 kV. During imaging the samples were maintained at -177 °C and pictures were taken using a CCD multiscan camera (Gatan).

Surface tension measurements
The surface tension measurements were performed to detect and characterize the formation of molecular aggregates of the surfactants. The water (degassed, Milli-Q water) solutions of the compounds were prepared by successive dilution of a concentrated sample, and then aged for 30 minutes before the determination of the surface tension. The measurements were performed with a Krüss K-12 automatic tensiometer (Hamburg, Germany) equipped with a platinum Wilhelmy plate, and for each sample five consecutive measurements, with a stability tuned to 0.1 $mN \cdot m^{-1}$, were done. The critical micellar concentrations (CMC) were obtained from the intersection of the linear parts of the surface tension versus logarithm of the concentration plots. The area (A, in $Å^2$) occupied per molecule adsorbed at the water/air interface was calculated from the equation $A=1016 / N_A \Gamma$, where N_A is Avogadro's number and Γ the surface excess concentration (mol/cm2). Γ was obtained from the Gibbs equation: $\Gamma = -(d\gamma/d \log C)/2.303nRT$, where $(d\gamma/d\log C)$ is the slope of the linear part of the graph obtained immediately below the CMC, and n is the number of molecular species in solution, that is, n = 2 for surfactant phosphine ligands and n=3 for the molybdenum metallosurfactants.

Fluorescence spectroscopy
The intrinsic fluorescence of the phenyl groups of the surfactant molecules allowed to monitor by fluorescence spectroscopy changes on their environment caused by variations of their state of aggregation. The emission spectra of the different molecules were obtained with PTI QuantaMaster spectrofluorimeter using a sample holder termostated at 25ºC and with magnetic stirring. The excitation wavelengths used were comprised from 250 to 305 nm, depending on the sample, in order to obtain a good signal to noise ratio. Samples were progressively diluted and at each concentration several consecutive scans were acquired till no variation of the shape and intensity of the spectra were observed. Usually, an equilibration time of about 30 minutes was needed for the highly concentrated samples, but in all the other cases it did not last more than 2 to 4 minutes.

Small Angle X-ray Scattering (SAXS)
SAXS patterns were recorded using a S3-MICRO (Hecus X-ray systems, Graz, Austria) coupled to a GENIX-Fox 3D X-ray source (Xenocs, Grenoble, France) working at 50 kV and 1 mA (λ =1.542 Å). The working q range was $0.1 \leq q \leq 6$ nm−1, and the temperature 25.0±0.1 °C, where $q = (4 \pi \sin\theta)/\lambda$ is the scattering wave vector

modulus, θ the scattering angle and λ the incident wavelength. For each experiment the scattering pattern was recorded as a sum of subscans to verify there was not sample evolution. The curves were fitted to intensity models obtained by either spherical step electronic density profiles or lamellar step electronic density profiles.[36] Our home-made fitting routines allow for convolution of the theoretical curves with our experimental detector width smearing function and use a Leverberg-Marquad scheme for minimization.[37] In the fitting we have let free the area per molecule A_m, the hydrophobic length L_c, and the hydrophilic length L_h. Using these, we have calculated the hydrophobic electron density ρ_c, the number of water molecules in the polar region N_w, and the hydrophilic electron density ρ_h. To do so we have set the number of electrons of the hydrophobic region as the total number of electrons of the molecule minus that of the polar head, which we have fixed as corresponding to the sulfonate group and one methylene.

Measurement of CO release

The CO release from the metallosurfactant molecules was measured by means of the mioglobine (Mb) assay,[38] which is based on the high affinity of this protein for the CO dissolved in an aqueous medium. A solution of reduced mioglobine (deoxy-Mb) 53 μM in phosphate biological saline buffer (PBS; previously degassed by bubbling N_2) at pH 7.4 was obtained by adding sodium dithionite at a final concentration of 1% w/w and, afterwards, bubbling N_2 again. For obtaining a spectrum between 250 and 650 nm a spectrophotometer cuvette was filled with an aliquot of this solution and capped to avoid any entrance of air. The obtained curve corresponded to a reference sample with no CO-bounded to Mb and showed a local maximum at 556 nm. For obtaining the spectrum of the totally CO-saturated Mb (that is, 53 μM of CO-Mb) an aliquot of the previous solution was intensely bubbled with CO. In this case the curve showed two local maxima located at 540 and 580 nm. Both spectra, from deoxy-Mb and CO-Mb, shared four isosbestic points at 510, 550, 570 and 585 nm. The release of CO from the samples was monitored by obtaining the spectra of an aliquot of the previously described deoxy-Mb solution containing the tested metallosurfactant at a concentration of 250 μM and at 37ºC. After correction of the spectra taking into account the isosbestic points, the concentration of CO-MB was quantified from the absorbance at 540 nm.

ASSOCIATED CONTENT

Supporting Information
The Supporting Information is available free of charge on the ACS Publications website at DOI:
Spectroscopic data for complexes **4**-**9**
Surface excess concentration and the estimated area per molecule for compounds **1**-**9**.
Molecular parameters of macromolecular aggregates obtained by SAXS for compounds **1**, **4** and **7**.
Excluded volume routine procedure.

AUTHOR INFORMATION

Corresponding Authors
* E-mail for J.S: joan.suades@uab.cat
* E-mail for R.B.-R.: ramon.barnadas@uab.cat

Notes

The authors declare no competing financial interest.

ACKNOWLEDGEMENTS

We acknowledge Mr. Jaume Caelles from the SAXS-WAXS service at IQAC for measurements. This research was supported by the Spanish MINECO and FEDER funds through the projects BIO2012-39682-C02-02 and MINECO-CTQ2013-41514-P.

REFERENCES

(1) (a) Scrimin, P.; Tecilla, P.; Tonellato, U.; Vendrame, T. *J. Org. Chem.*, **1989**, *54*, 5988-5991. (b) Ghirlanda, G.; Scrimin, P.; Kaifer, A. E.; Echegoyen, L. A. *Langmuir*, **1996**, *12*, 3695-3701. (c) Fallis, I. A.; Griffiths, P. C.; Griffiths, P. M.; Hibbs, D. E.; Hursthouse, M. B.; Winnington, A. L. *Chem. Commun.*, **1998**, *6*, 665-666.

(2) Valls, E.; Solsona, A.; Suades, J.; Mathieu, R.; Comelles, F.; López-Iglesias, C. *Organometallics*, **2002**, *21*, 2473-2480.

(3) Griffiths, P. C.; Fallis, I. A.; Chuenpratoom, T.; Watanesk, R. *Adv. Colloid Interface Sci.*, **2006**, *122*, 107-117.

(4) (a) Fell, B.; Pagadogianakis, G. *J. Mol. Catal.* **1991**, *66*, 143-154. (b) Ding, H.; Hanson, B. E.; Bakos, J. *Angew. Chem. Int. Ed.* **1995**, *34*, 1645-1647. (c) Gulyas, H.; Arva, P.; Bakos, J. *Chem. Commun.* **1997**, *24*, 2385-2386. (d) Goedheijt, M. S.; Hanson, B. E.; Reek, J. N. H.; Kamer, P. C. J.; van Leeuwen, P. W. N. M. *J. Am. Chem. Soc.* **2000**, *122*, 1650-1657.

(5) Parera, E; Comelles, F.; Barnadas, R.; Suades, J. *Langmuir*, **2010**, *26*, 743-751.

(6) (a) Bhattacharya, S.; Kumari, N. *Coord. Chem. Rev*. **2009**, *253*, 2133-2149. (b) Mancin, F.; Scrimin, P.; Tecilla, P.; Tonellato, U. *Coord. Chem. Rev*. **2009**, *253*, 2150-2165.(c) Zhang, J.; Meng, X.; Zeng, X.; Yu, X. *Coord. Chem. Rev*. **2009**, *253*, 2166-2177. (d) Li, J.; Tang, Y.; Wang, Q.; Li, X.; Cun, L.; Zhang, X.; Zhu, J.; Li, L.; Deng, J. *J. Am. Chem. Soc*. **2012**, *134*, 18522-18525. (e) Chakravarthy, R. D.; Ramkumar, V.; Chand, D. K. *Green Chem*. **2014**, *16*, 2190-2196.

(7) (a) Amos, K. E.; Brooks, N. J.; King, N. C.; Xie, S.; Canales-Vázquez, J.; Danks, M. J.; Jervis, H. B.; Zhou, W.; Seddon, J. M.; Bruce, D. W. *J. Mater. Chem*., **2008**, *18*, 5282-5292. (b) Botelho, M.; Fernandez-Hernandez, J.; Branquinho de Queiroz, T.; Eckert, H.; De Cola, L.; de Camargo, A. *J. Mater. Chem.* **2011**, *21*, 8829-8834. (c) Hondow, N.; Harowfield, J.; Koutsantonis, G.; Nealon, G.; Saunders, M. *Micropor. Mesopor. Mat*. **2012**, *151*, 264-270.

(8) (a) Donnio, B. *Curr. Opin. Colloid Interface Sci*., **2002**, *7*, 371-394. (b) Iida, M.; Inoue, M.; Tanase, T.; Takeuchi, T.; Sugibayashi, M.; Ohta, K. *Eur. J. Inorg. Chem*., **2004**, *19*, 3920-3929. (c) Cardinaels, T.; Ramaekers, J.; Driesen, K.; Nockemann, P.; Van Hecke, K.; Van Meervelt, L.; Goderis, B.; Binnemans, K. *Inorg. Chem.*, **2009**, *48*, 2490-2499.

(9) (a) Nazeeruddin, M. K.; Zakeeruddin, S. M.; Lagref, J. J.; Liska, P.; Comte, P.; Barolo, C.; Viscardi, G.; Schenk, K.; Graetzel, M. *Coord. Chem. Rev*., **2004**, *248*, 1317-1328. (b) Jayathilake, H. D.; Driscoll, J. A.; Bordenyuk, A. N.; Wu, L.; da Rocha, S. R. P.; Verani, C. N.; Benderskii, A. V. *Langmuir*, **2009**, *25*, 6880-6886. (c) Lesh, F. D.; Allard, M. M.; Shanmugam, R.; Hryhorczuk, L. M.; Endicott, J. F.; Schlegel, H. B.; Verani, C. N. *Inorg. Chem.* **2011**, *50*, 969-977. (d) Mauro, M.; De Paoli, G.; Otter, M.; Donghi, D.; D'Alfonso, G.; De Cola, L. *Dalton Trans*. **2011**, *40*, 12106-12116. (e) Fernandez-Hernandez, J. M.; De Cola, L.; Bolink, H. J.; Clemente-Leon, M.; Coronado, E.; Forment-Aliaga, A.; Lopez-Munoz, A.; Repetto, D. *Langmuir* **2014**, *30*, 14021-14029.

(10) Joy, S.; Pal, Prabir; Mondal, T. K.; Talapatra, G. B.; Goswami, S. *Chem. Eur. J*. **2012**, *18*, 1761-1771.

(11) (a) Iida, M.; Baba, C.; Inoue, M.; Yoshida, H.; Taguchi, E.; Furusho, H. *Chem. Eur. J*., **2008**, *14*, 5047-5056. (b) Ye, S.; Liu, Y.;

Chen, S.; Liang, S.; McHale, R.; Ghasdian, N.; Lu, Y.; Wang, X. *Chem. Commun*. **2011**, *47*, 6831-6833. (c) Kaur, R.; Mehta, S. K. *Coord. Chem. Rev*. **2014**, *262*, 37-54.

(12) Mechler, A.; Stringer, B. D.; Mubin, M. S. H.; Doeven, E. H.; Phillips, N. W.; Rudd-Schmidt, J.; Hogan, C. F. *BBA-Biomembranes* **2014**, *1838*, 2939-2946.

(13) Aiad, Ismail A.; Badawi, Abdelfatah M.; El-Sukkary, Mohammed M.; El-Sawy, Abdallah A.; Adawy, Ahmed I. *J. Surfactants Deterg*. **2012**, *15*, 223-234.

(14) (a) Vaccaro, M.; Mangiapia, G.; Radulescu, A.; Schillén, K.; D'Errico, G.; Morelli, G.; Paduano, L. *Soft Matter*, **2009**, *5*, 2504-2512. (b) Gong, P.; Chen, Z.; Chen, Y.; Wang, W.; Wang, X.; Hu, A. *Chem. Commun*., **2011**, *47*, 4240-4242. (c) Chen, Y.; Zhu, Q.; Tian, Y.; Tang, W.; Pan, F.; Xiong, R.; Yuan, Y.; Hu, A. *Polym. Chem*. **2015**, *6*, 1521-1526.

(15) (a) Cheng, Z.; Ren, B.; Gao, M.; Liu, X.; Tong, Z. *Macromolecules* **2007**, *40*, 7638-7643. (b) Tsuchiya, K.; Yajima, H.; Sakai, H.; Abe, M. *Electrical Phenomena at Interfaces and Biointerfaces*, Ohshima, H. Editor, John Wiley & Sons Inc.: Hoboken, **2012**, pp 567-582.

(16) Thanasekaran, P.; Wu, J.Y.; Manimaran, B.; Rajendran, T.; Chang, I. J.; Rajagopal, S.; Lee, G. H.; Peng, S.M.; Lu, K. L. *J. Phys. Chem. A*, **2007**, *111*, 10953-10960.

(17) (a) Griffiths, P.C., Fallis, I.A., Chuenpratoom, T.; Watanesk, R. *Adv. Colloid Interface Sci*. **2006**, *122*, 107–117. (b) Tate Owen, T., Butler, A. Coord. Chem. Rev. **2011**, *255*, 678–687.

(18) Johnson, T. R.; Mann, B. E.; Clark, J. E.; Foresti, R.; Green, C. J.; Motterlini R. *Angew. Chem. Int. Ed*. **2003**, *42*, 3722 – 3729.

(19) (a)Mann, B. E. *Topics in Organometallic Chemistry* **2010**, *32*(Medicinal Organometallic Chemistry), 247-285. (b) Tavares, A. F. N.; Nobre, L. S.; Saraiva, L. M. *FEMS Microbiol. Lett*. **2012**, *336*, 1-10. (c) Gonzales, M. A.; Mascharak, P. K. *J. Inorg. Biochem*. **2014**, *133*, 127-135. (d) Heinemann, S. H.; Hoshi, T.; Westerhausen, M.; Schiller, A. *Chem. Commun*. **2014**, *50*, 3644-3660. (e) Garcia-Gallego, S.; Bernardes, G. J. L. *Angew. Chem. Int. Ed*. **2014**, *53*, 9712-9721. (f) Marhenke, J.; Trevino, K.; Works, C. *Coord. Chem. Rev*. **2015**, http://dx.doi.org/10.1016/j.ccr.2015.02.017.

(20) Hasegawa, U.; van der Vlies, A.J.; Simeoni, E.; Wandrey, C.; Hubbell J. A. *J. Am. Chem. Soc*. **2010**, *132*, 18273–18280.

(21) Parera, E.; Comelles, F.; Barnadas R.; Suades J. *Chem. Commun*. **2011**, *47*, 4460–4462.

(22) Larpent, C.; Patin, H. *Appl. Organomet. Chem*., **1987**, *1*, 529-534.

(23) van Assema, S. G. A.; de Kanter, F. J. J.; Schakel, M.; Lammertsma, K. *Organometallics* **2006**, *25*, 5286-5291.

(24) Cotton, F. A.; Kraihanzel, C. S. *J. Am. Chem. Soc*., **1962**, *84*, 4432-4438.

(25) Darensbourg, D. J.; Kump, R. L. *Inorg. Chem*., **1978**, *17*, 2680-2682.

(26) Darensbourg, D. J.; Bischoff, C. J. *Inorg. Chem.*, **1993**, *32*, 47-53.

(27) Alyea, E. C.; Song, S. *Inorg. Chem*., **1995**, *34*, 3864-3873.

(28) (a) Matsuoka, K.; Moroi, Y. *Biochim. Biophys. Acta* **2002**, *1580*, 189-199. (b) Barnadas-Rodríguez, R.; Estelrich, J. *J. Phys. Chem. B* **2009**, *113*, 1972-1982. (c) Barnadas-Rodríguez, R.; Cladera, J. *Langmuir* **2015**, *31*, 8980−8988.

(29) Hadgiivanova, R.; Diamant, H. *J. Chem. Phys.* **2009**, *130*, 114901-1/5.

(30) (a) Menger, F. M.; Shi, L.; Rizvi, S. A. A. *J. Am. Chem. Soc*., **2009**, *131*, 10380-10381. (b) Menger, F. M.; Shi, L.; Rizvi, S. A. A. *Langmuir*, **2010**, *26*, 1588-1589.

(31) (a) Israelachvili, J.; Mitchell, D. J.; Ninham, B. W. *Biochim Biophys. Acta*. **1977,** *470*, 185-201. (b) Nagarajan, R. *Langmuir* **2002**, *18*, 31-38.

(32) Barnadas, R.; Sabés, M. *Meth. Enzymol*. **2003**, *367*, 28-46.

(33) Xu, H.; Li, P.X.; Ma,

K.; Thomas, R.K.; Penfold, J.; Lu, J.R. *Langmuir*, **2013**, *29*, 9335–9351.

(34) (a) Paquette, R. G.; Lingafelter, E. C.; Tarta, H.V. *J. Am. Chem. Soc*., **1943**, *65*, 686–692. (b) Wright, K.A.; Tartar, H.V. *J. Am. Chem. Soc*., **1939**, *61*, 544–549. (c) A. Pinazo, A.; Pérez, L.; Lozano, M.; Angelet, M.; Infante, M.R.; Vinardell, M.P.; Pons, R. *J. Phys. Chem. B*, **2008**, *112*, 8578–8585.

(35) Schatzschneider, U. *Inorganica Chimica Acta*, **2011**, *374*, 19-23.

(36) Pedersen, J.S. *Adv. Colloid Interface Sci*. **1997**, *70*, 171-210.

(37) Morros, J.; Infante, M.R.; Pons, R. *Soft Matter*, **2012**, *8*, 11353-11362.

(38) Strinitz, F.; Trautner, P.; Pfeiffer, H.; Schatzschneider, U.; Burzlaff, N. *Tetrahedron*, **2015**, *71*, 2951–2954.

SUPPORTING INFORMATION

Supramolecular arrangement of molybdenum carbonyl metallosurfactants with CO releasing properties

Elisabet Parera,[†,§] Maribel Marín-García,[†,‡] Ramon Pons,[‖] Francesc Comelles,[‖] Joan Suades*[,§] and Ramon Barnadas-Rodríguez*[,‡]

[‡]Unitat de Biofísica/Centre d'Estudis en Biofísica, Facultat de Medicina, Departament de Bioquímica i Biologia Molecular, Universitat Autònoma de Barcelona. 08193 Cerdanyola del Vallès, Spain

[§]Departament de Química, Edifici C, Universitat Autònoma de Barcelona, 08193 Cerdanyola del Vallès, Spain

[‖]Institut de Química Avançada de Catalunya, IQAC-CSIC, Jordi Girona, 18-26, 08034 Barcelona, Spain

[†] Both authors have contributed equally to this work.

Corresponding Authors

* E-mail for J.S: joan.suades@uab.cat

* E-mail for R.B.-R.: ramon.barnadas@uab.cat

Supporting Information 1

Spectroscopic data for complexes 4, 5 and 6.

a) IR spectroscopy (νCO region, spectra in CH_2Cl_2)

Complex	ν_{CO} (cm^{-1})
4	2073, 1990, 1945
5	2072, 1988, 1944
6	2071, 1988, 1943

Complex **4**

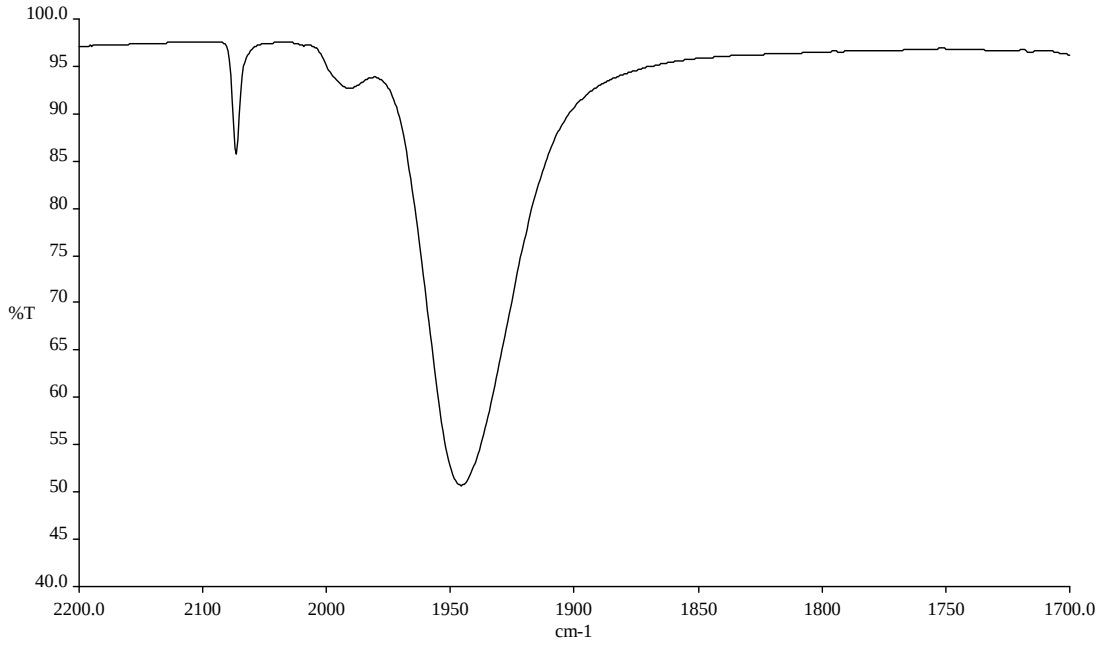

Complex **5**

Complex **6**

b) ^{31}P NMR data (spectra in methanol-d^4)

Complex	δ (ppm)
4	26.7 (s)
5	27.2 (s)
6	27.4 (s)

Complex **4**

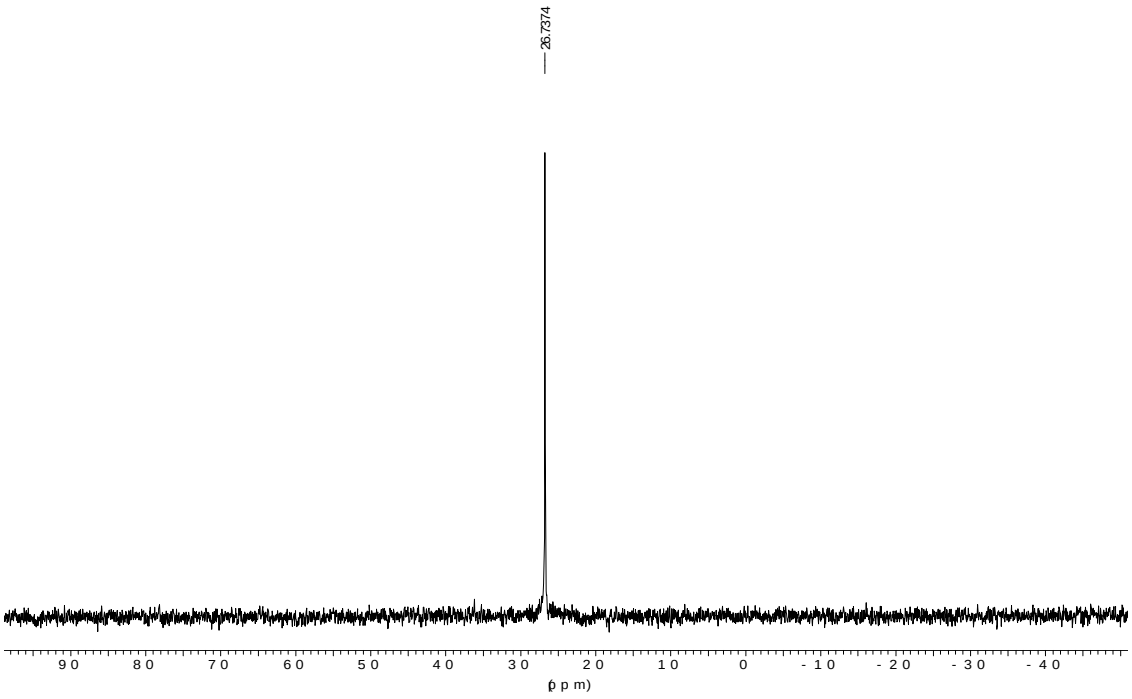

Complex **5**

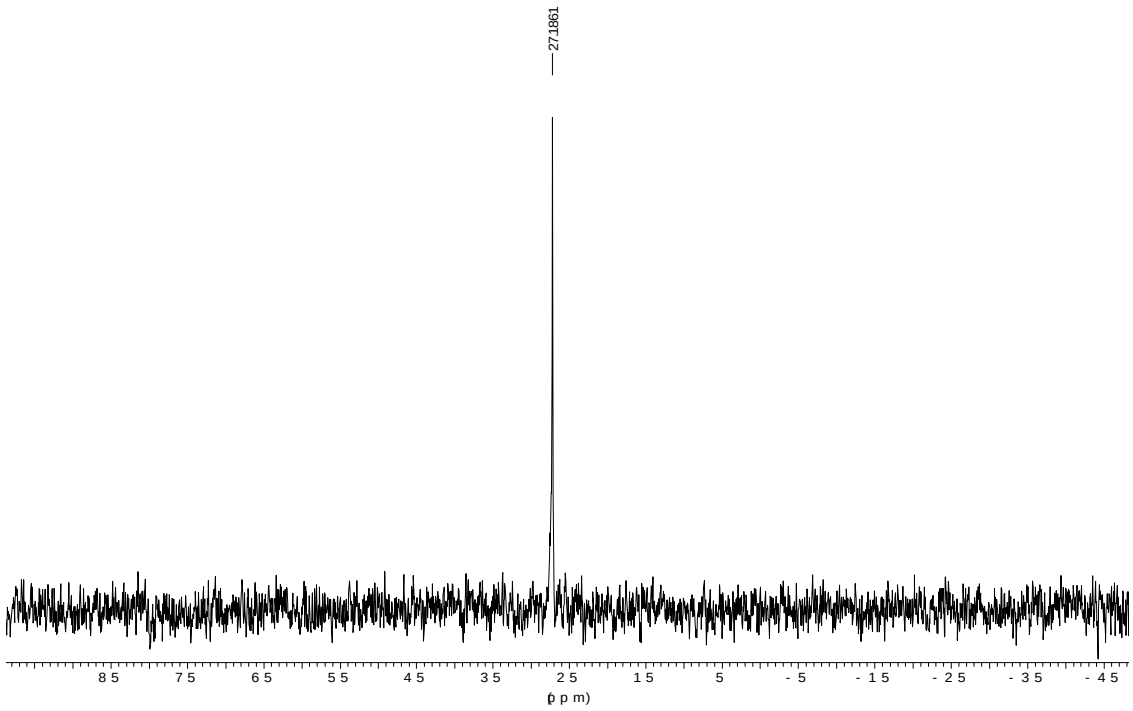

Complex **6**

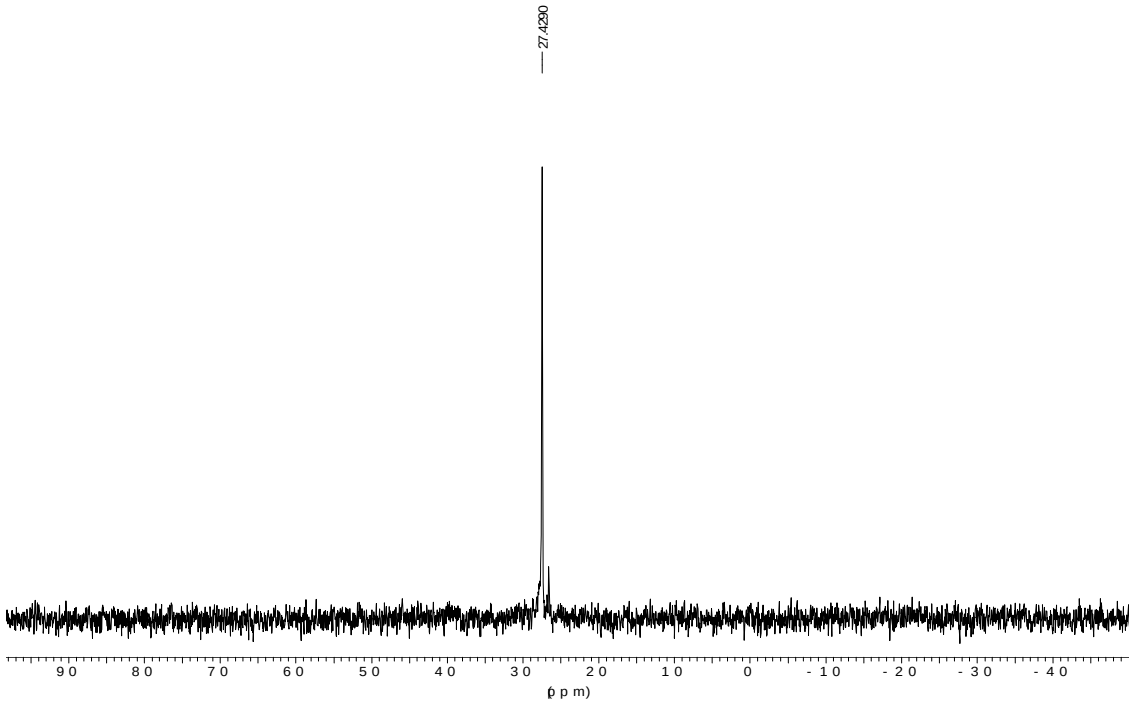

c) ^{1}H NMR data (spectra in methanol-d^{4})

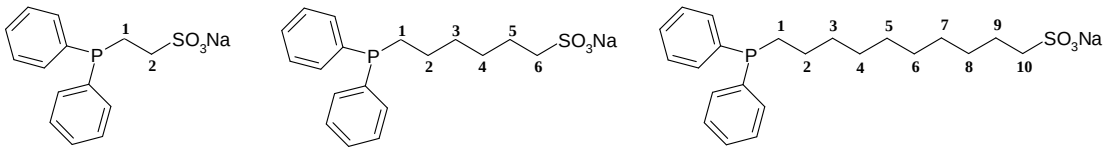

(numbering scheme used for NMR assignments)

Complex 4

Assignation	δ (ppm)	Integration
Ph	7.69 – 7.45 (m)	10H
2	3.00 – 2.89 (m)	2H
1	2.73 – 2.62 (m)	2H

Complex 5

Assignation	δ (ppm)	Integration
Ph	7.68 – 7.42 (m)	10H
6	2.80 – 2.70 (m)	2H
1	2.56 – 2.41 (m)	2H
5	1.82 – 1.68 (m)	2H
2 - 4	1.49 – 1.32 (m)	6H

Complex 6

Assignation	δ (ppm)	Integration
Ph	7.45 – 7.27 (m)	10H
10	2.70 – 2.63 (m)	2H
1	2.39 – 2.31 (m)	2H
9	1.71 – 1.59 (m)	2H
2 - 8	1.33 – 1.05 (m)	14H

Complex **4**

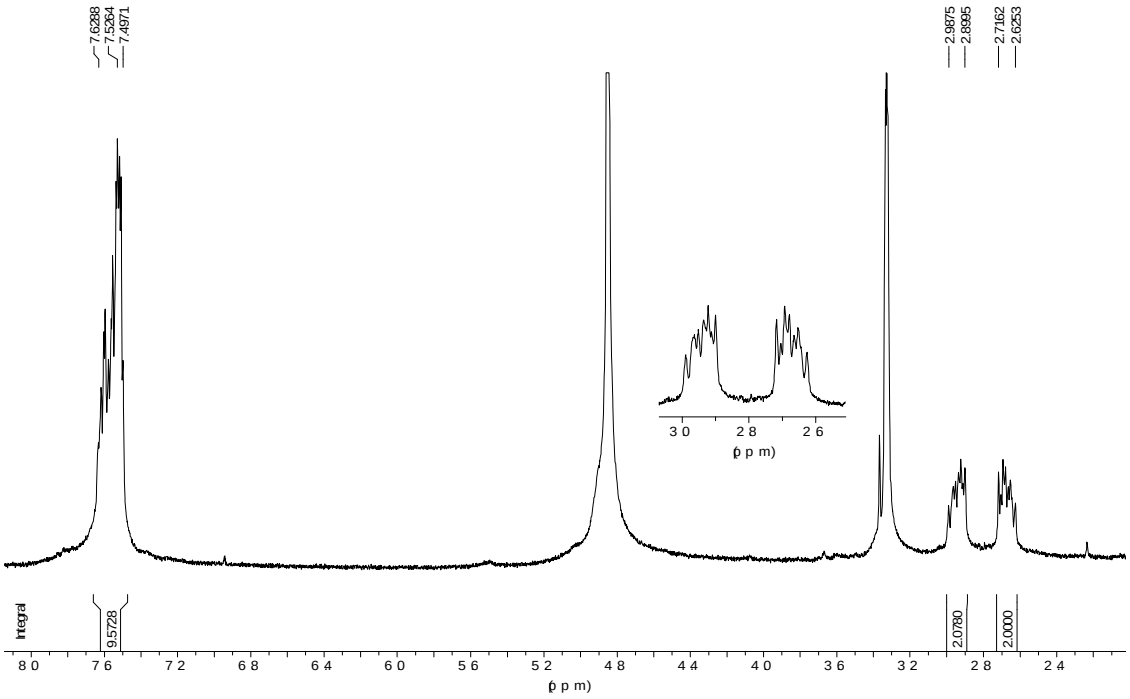

Complex **5**

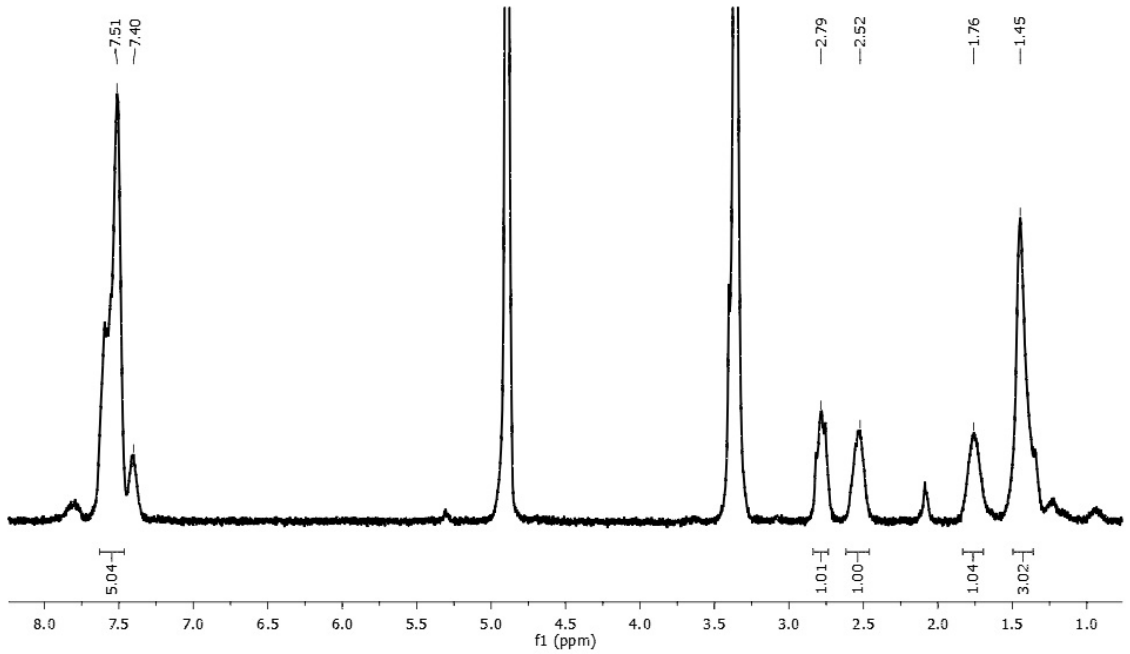

Complex **6**

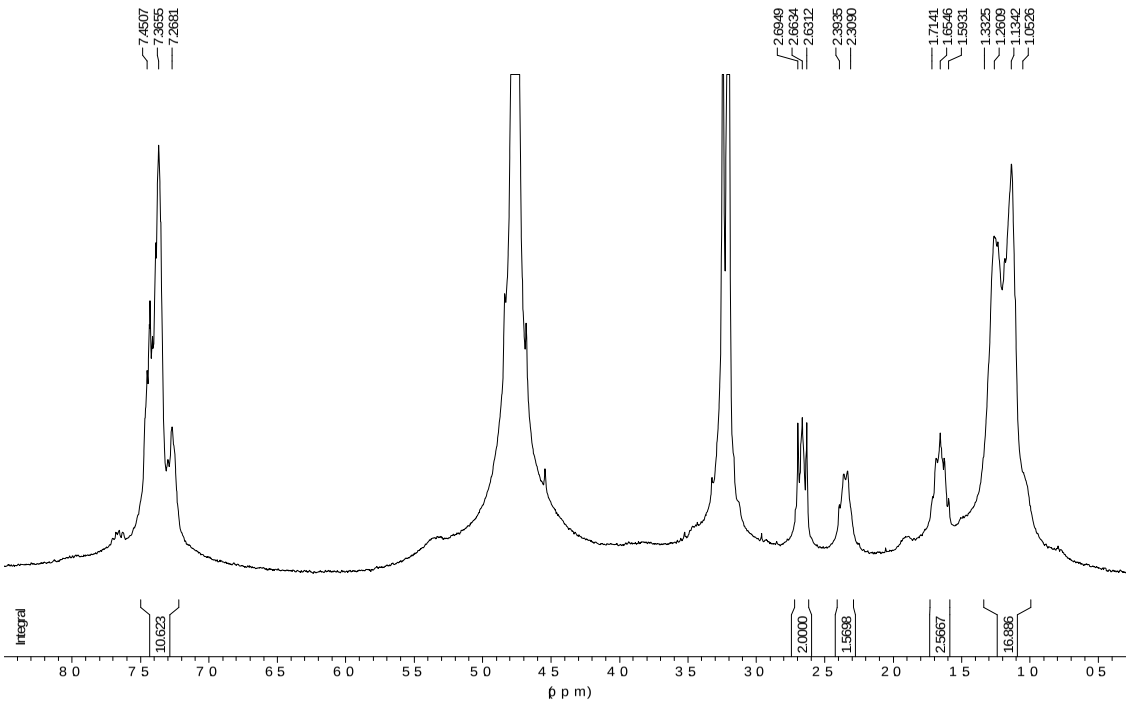
7.4507
7.3655
7.2681
2.6949
2.6634
2.6312
2.3935
2.3090
1.7141
1.6546
1.5931
1.3325
1.2609
1.1342
1.0526
Integral
10.623
2.0000
1.5698
2.5667
16.886
80 75 70 65 60 55 50 45 40 35 30 25 20 15 10 05
(p p m)

Spectroscopic data for complexes 7, 8 and 9.

a) IR spectroscopy (νCO region, spectra in CH_2Cl_2)

Complex	ν_{CO} (cm^{-1})
7	2020, 1925, 1897
8	2015, 1914, 1896, 1868
9	2018, 1917, 1900, 1875

Complex **7**

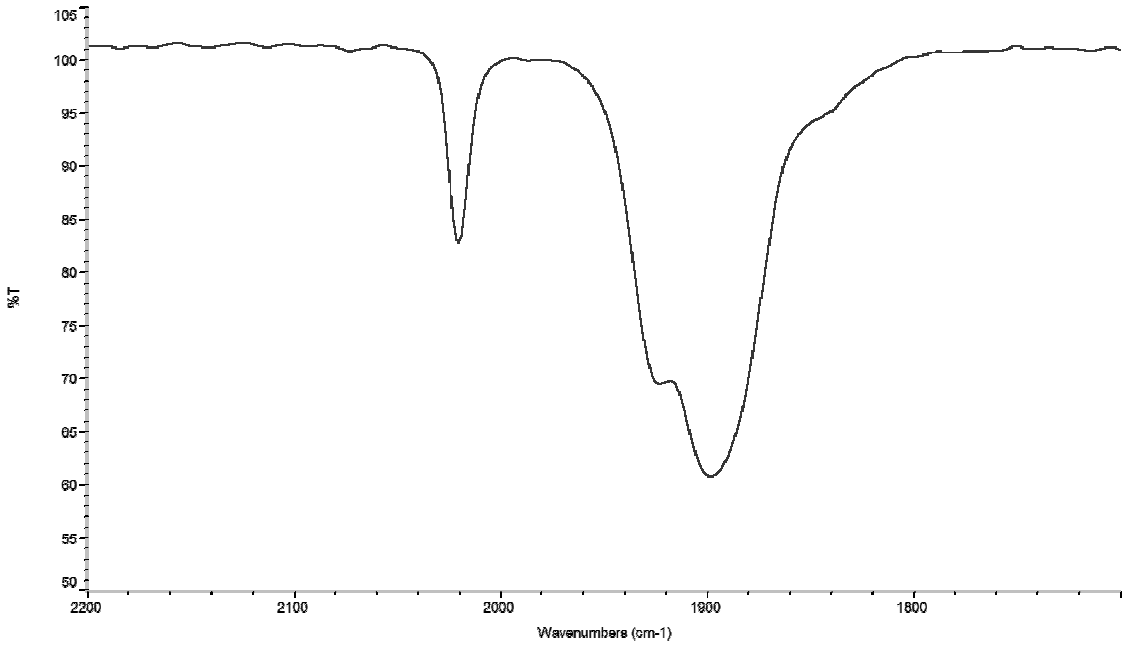

Complex **8**

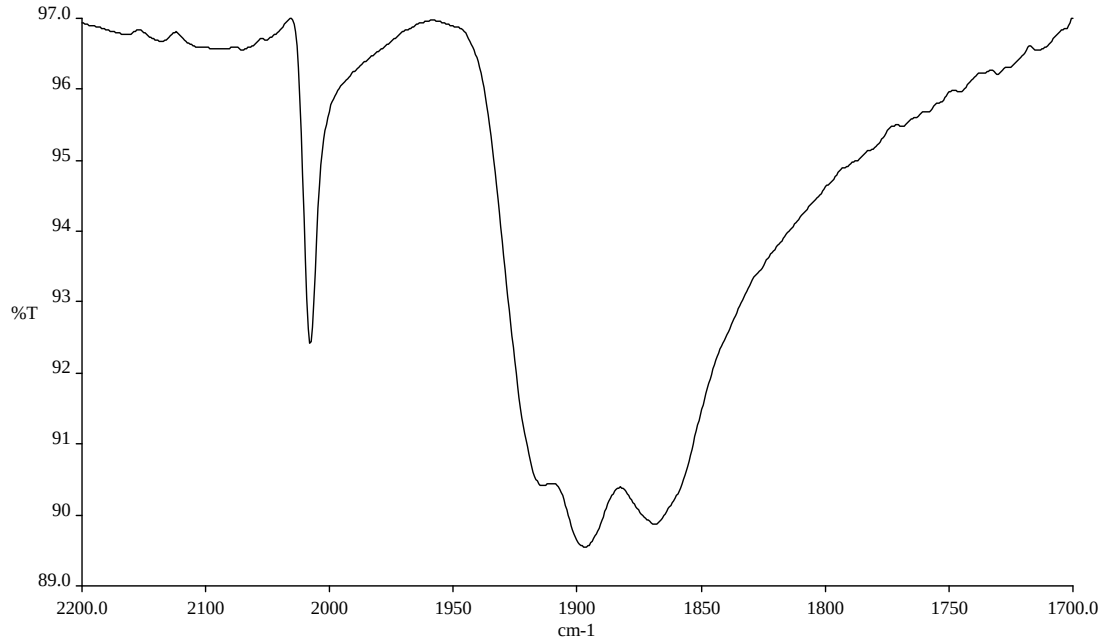

Complex **9**

b) ^{31}P NMR data (spectra in methanol-d^4)

Complex	δ (ppm)
7	25.6 (s)
8	26.3 (s)
9	26.5 (s)

Complex **7**

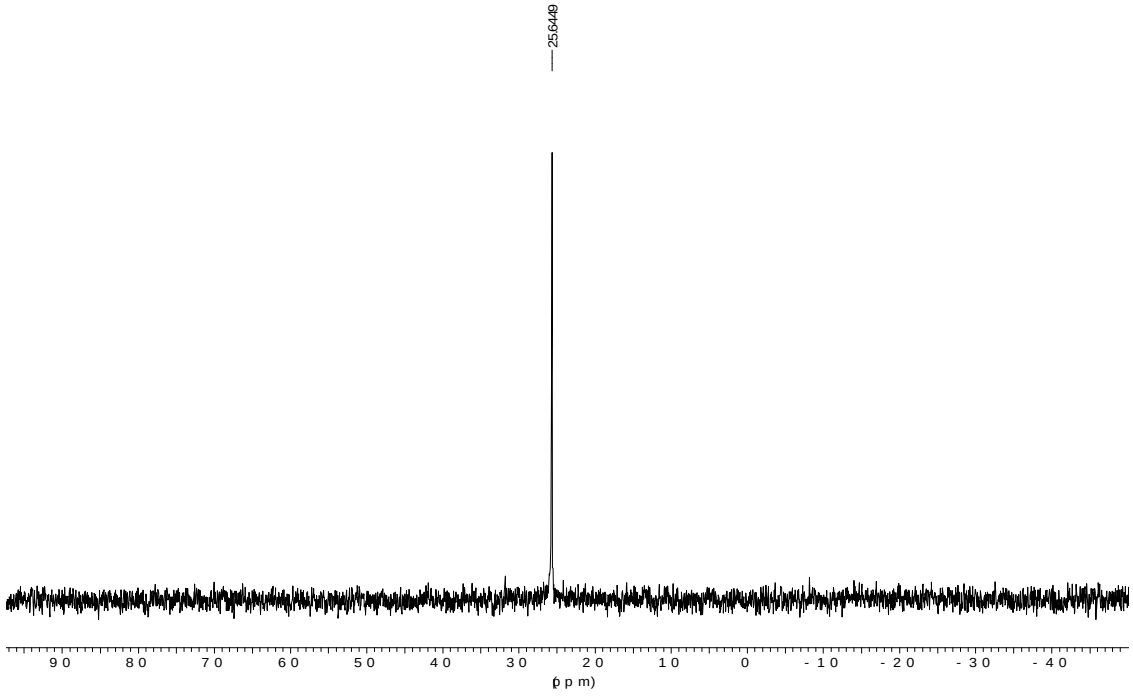

Complex **8**

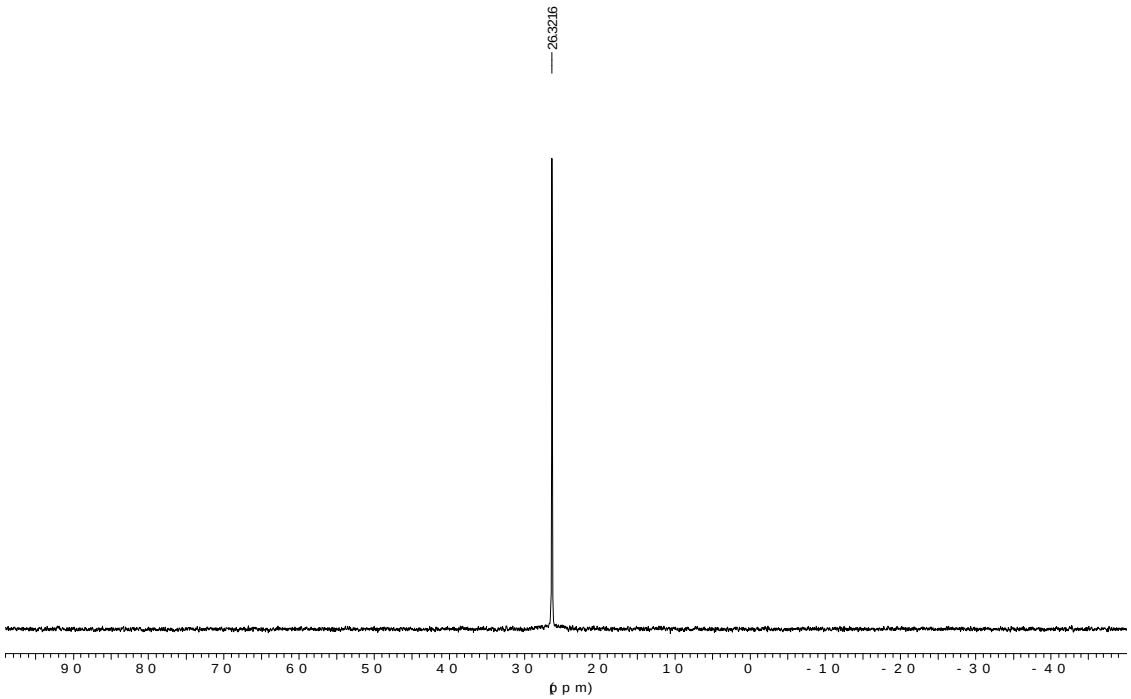

Complex **9**

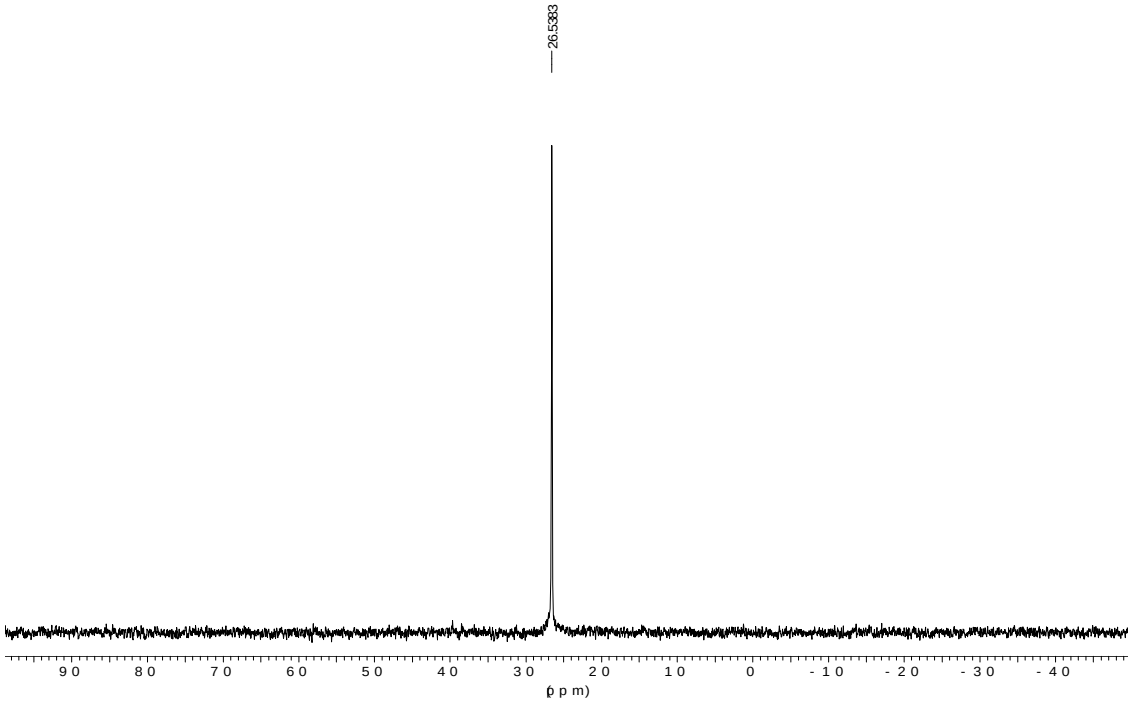

c) ^{1}H NMR data (spectra in methanol-d^{4})

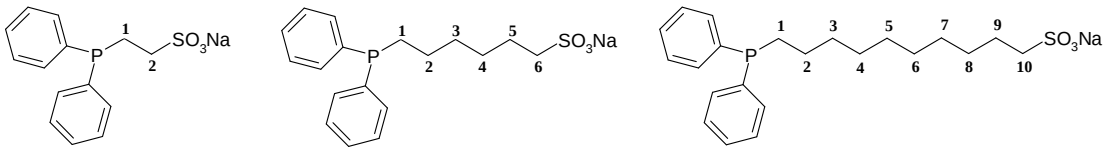

(numbering scheme used for NMR assignments)

Complex 7

Assignation	δ (ppm)	Integration
Ph	7.90 – 7.24 (m)	20H
2	2.84 – 2.69 (m)	4H
1	2.62 – 2.43 (m)	4H

Complex 8

Assignation	δ (ppm)	Integration
Ph	7.41 – 7.31 (m)	20H
6	2.73 – 2.66 (m)	4H
1	2.08 – 2.00 (m)	4H
5	1.69 – 1.59 (m)	4H
3, 4	1.25 – 1.16 (m)	8H
2	1.16 – 1.07 (m)	4H

Complex 9

Assignation	δ (ppm)	Integration
Ph	7.49 – 7.27 (m)	20H
10	2.81 – 2.73 (m)	4H
1	2.08 – 1.97 (m)	4H
9	1.82 – 1.70 (m)	4H
8	1.47 – 1.31 (m)	4H
2-7	1.31 – 1.01 (m)	28H

Complex **7**

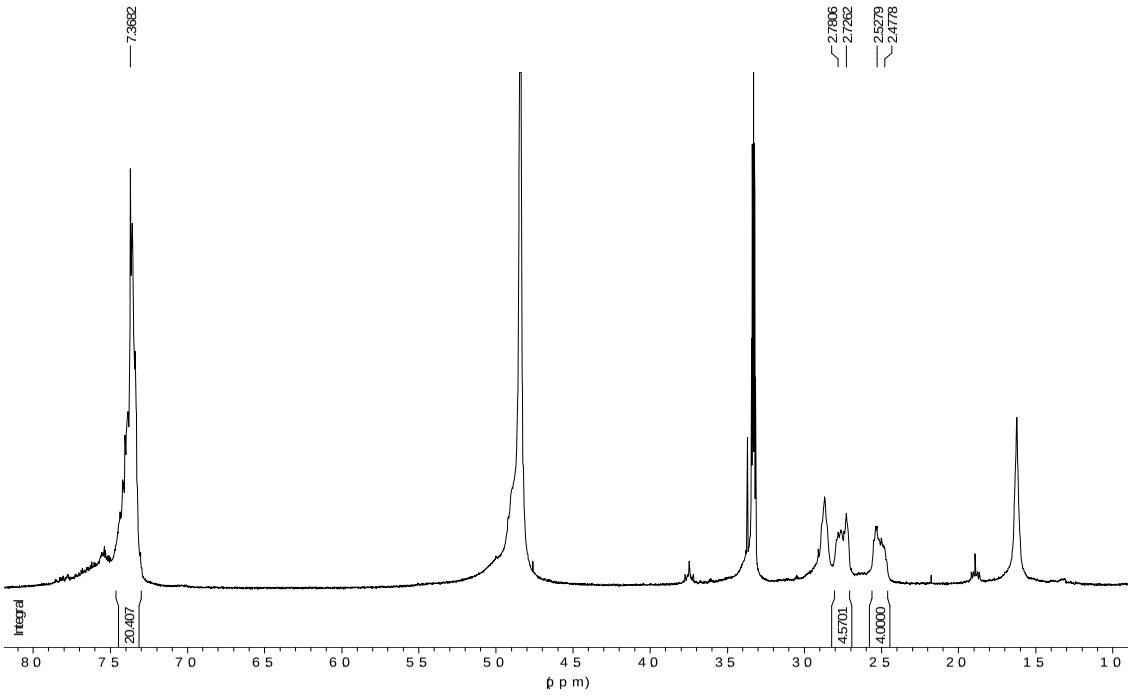

Complex **8**

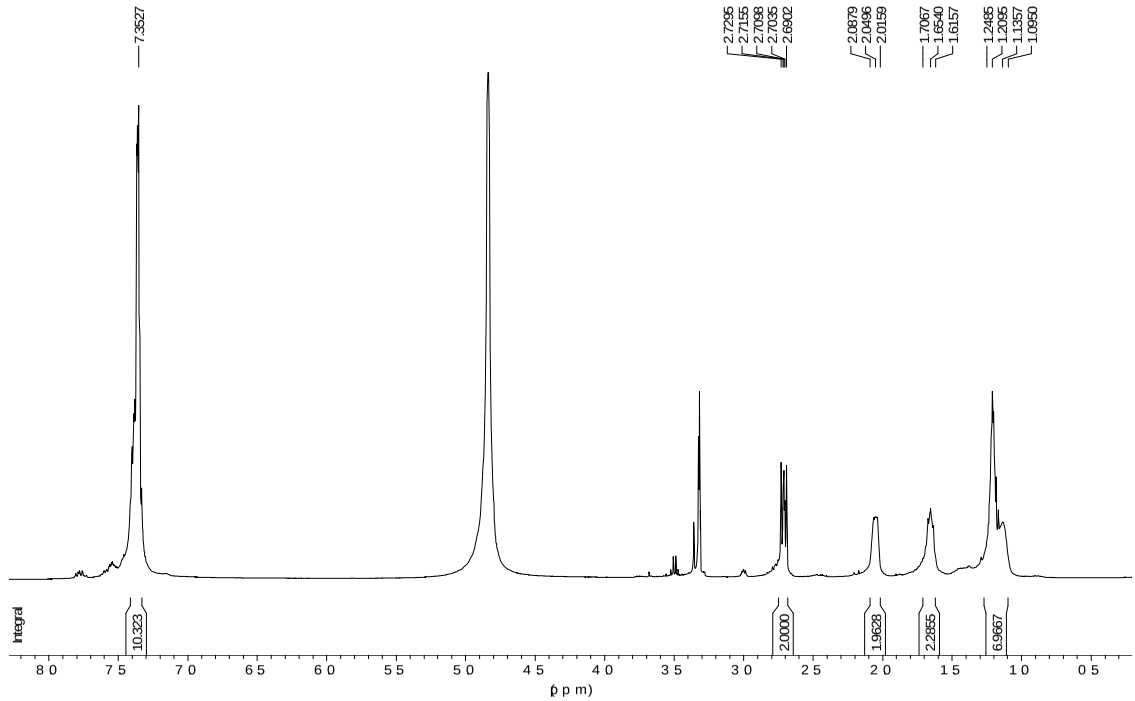

Complex **9**

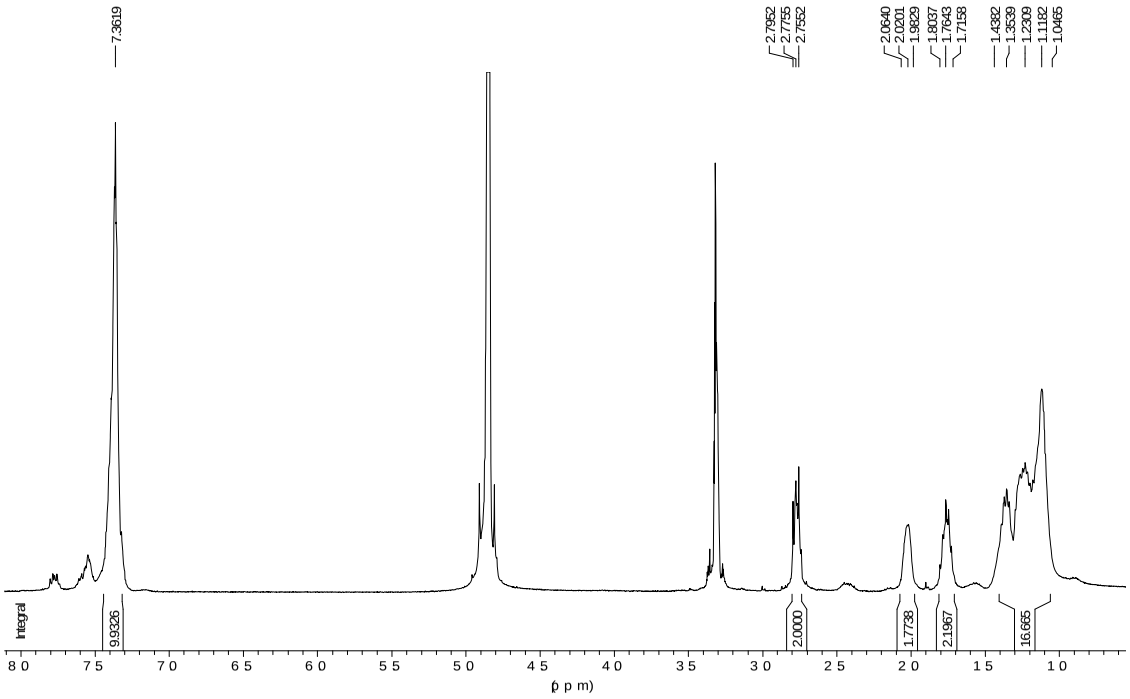
7.3619
2.7952
2.7755
2.7552
2.0640
2.0201
1.9829
1.8037
1.7643
1.7158
1.4382
1.3539
1.2309
1.1182
1.0465
Integral
9.9326
2.0000
1.7738
2.1957
16.665
80 75 70 65 60 55 50 45 40 35 30 25 20 15 10
(p p m)

c) ^{13}C NMR data (spectra in methanol-d^4)

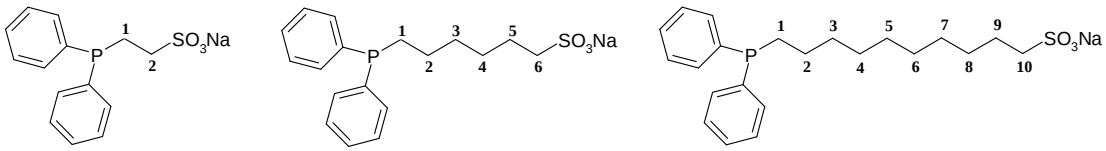

(numbering scheme used for NMR assignments)

Complex 7

Assignation	δ (ppm)	Multiplicity	J (Hz)
C≡O $_{ip}$	214.8	AXX' (3 lines)	$^2J_{C-P} + {}^2J_{C-P'} = 15.8$
C≡O $_{oop}$	209.3	AXX' (3 lines)	$^2J_{C-P} + {}^2J_{C-P'} = 18.9$
2	46.4	Singlet	---
1	28.3	AXX' (3 lines)	$^1J_{C-P} + {}^3J_{C-P'} = 20.42$

Complex 8

Assignation	δ (ppm)	Multiplicity	J (Hz)
C≡O $_{ip}$	215.3	AXX' (3 lines)	$^2J_{C-P} + {}^2J_{C-P'} = 15.91$
C≡O $_{oop}$	210.0	AXX' (3 lines)	$^2J_{C-P} + {}^2J_{C-P'} = 18.70$
6	51.0	Singlet	---
1	32.2	AXX' (3 lines)	$^1J_{C-P} + {}^3J_{C-P'} = 21.65$
3	30.3	AXX' (3 lines)	$^2J_{C-P} + {}^4J_{C-P'} = 12.77$
4	28.0	Singlet	---
5	24.4	Singlet	---
2	23.9	Singlet	---

Complex 9

Assignation	δ (ppm)	Multiplicity	J (Hz)
C≡O $_{ip}$	215.3	AXX' (3 lines)	$^{2}J_{C-P} + {}^{2}J_{C-P'} = 16.03$
C≡O $_{oop}$	210.0	AXX' (3 lines)	$^{2}J_{C-P} + {}^{2}J_{C-P'} = 19.40$
10	51.3	Singlet	---
1	32.2	AXX' (3 lines)	$^{1}J_{C-P} + {}^{3}J_{C-P'} = 21.64$
3	30.3	AXX' (3 lines)	$^{2}J_{C-P} + {}^{4}J_{C-P'} = 12.47$
4-7	28.9	Singlet	---
	28.9	Singlet	---
	28.7	Singlet	---
	28.6	Singlet	---
8	28.3	Singlet	---
9	24.5	Singlet	---
2	23.7	Singlet	---

Complex **7**

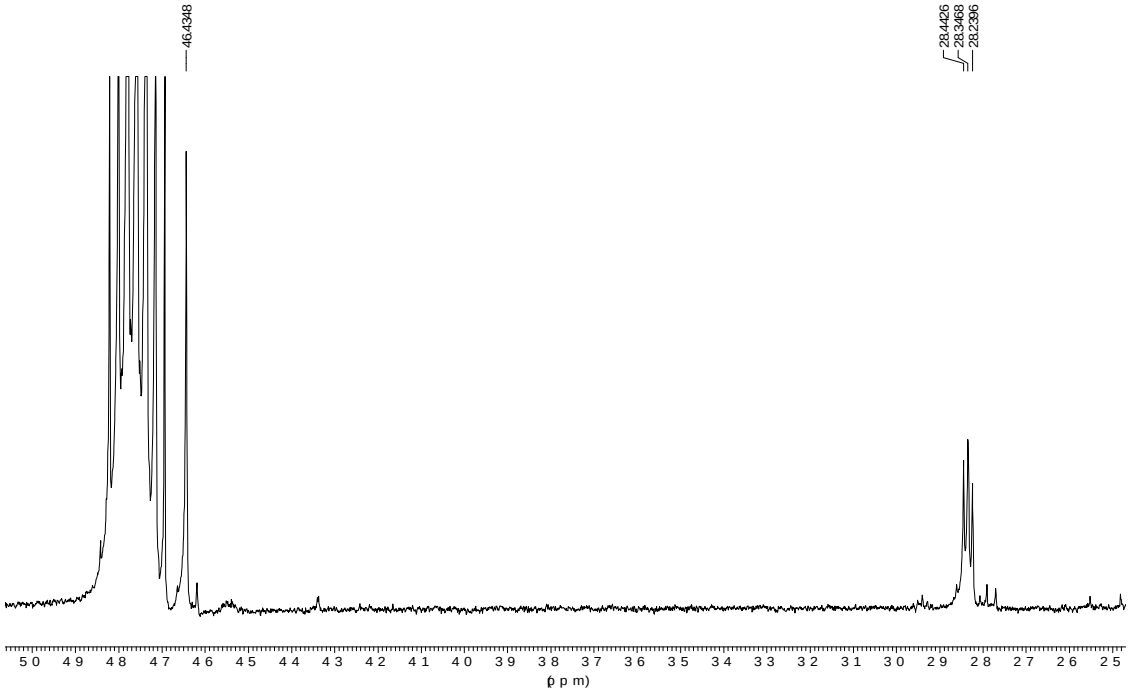

$^{13}C\{^{1}H\}$-RMN of **7** (aliphatic region)

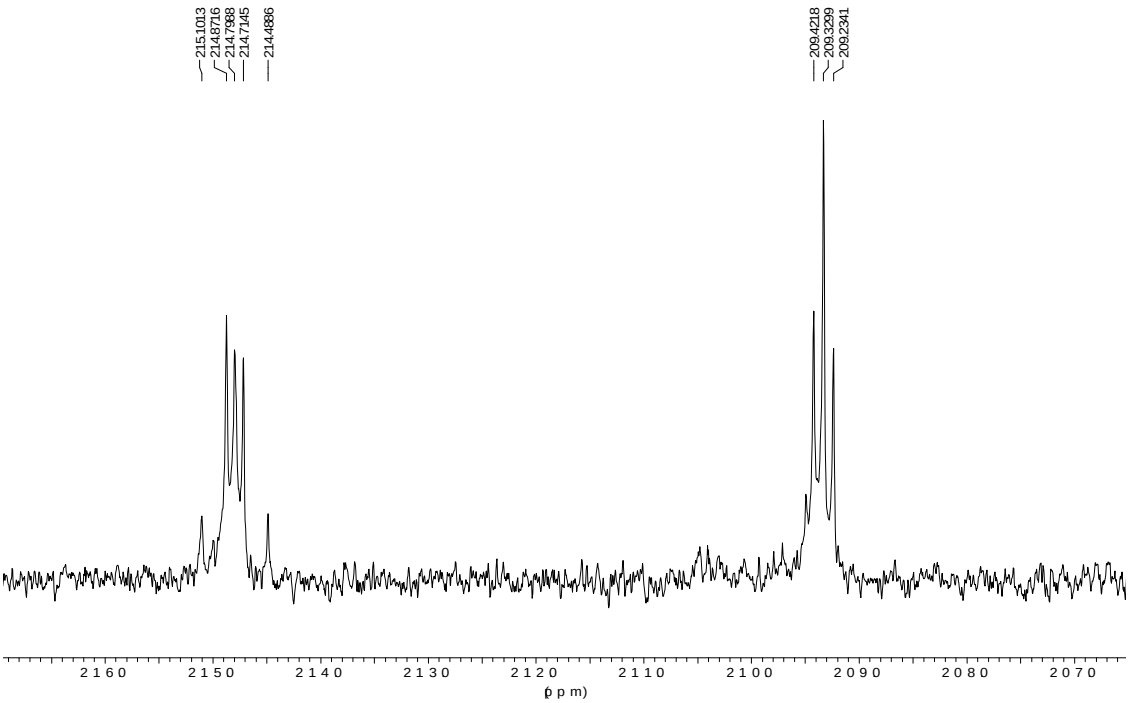

$^{13}C\{^{1}H\}$-RMN of **7** (carbonyl region)

Complex **8**

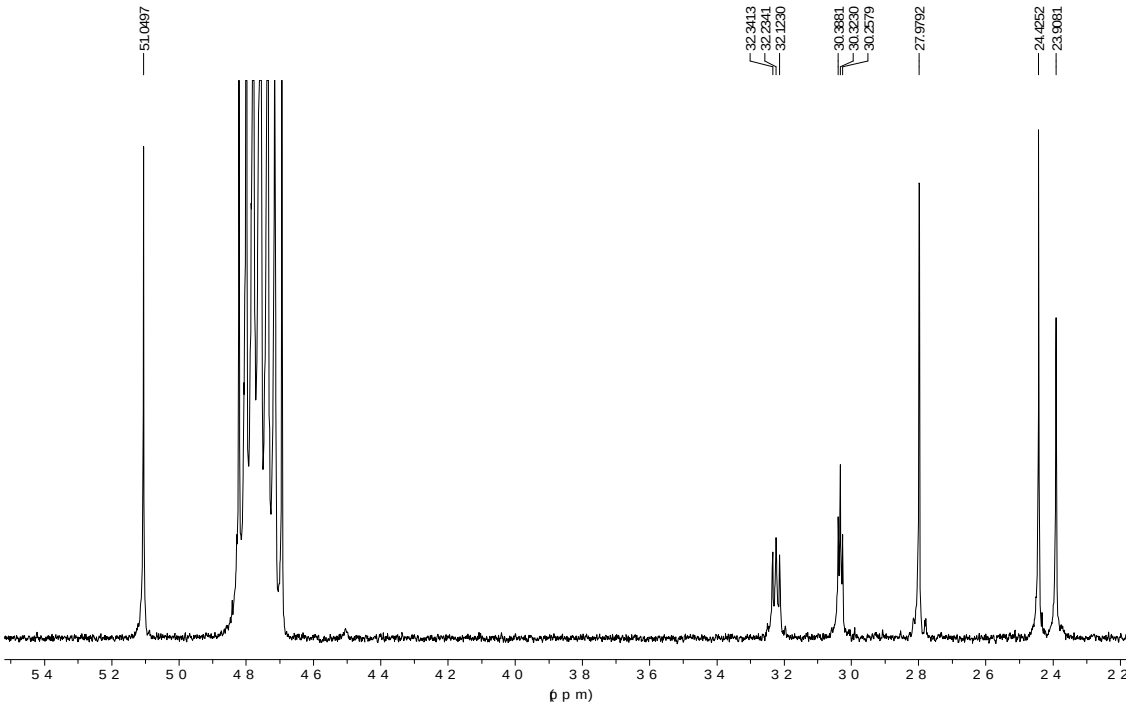

$^{13}C\{^{1}H\}$-RMN of **8** (aliphatic region)

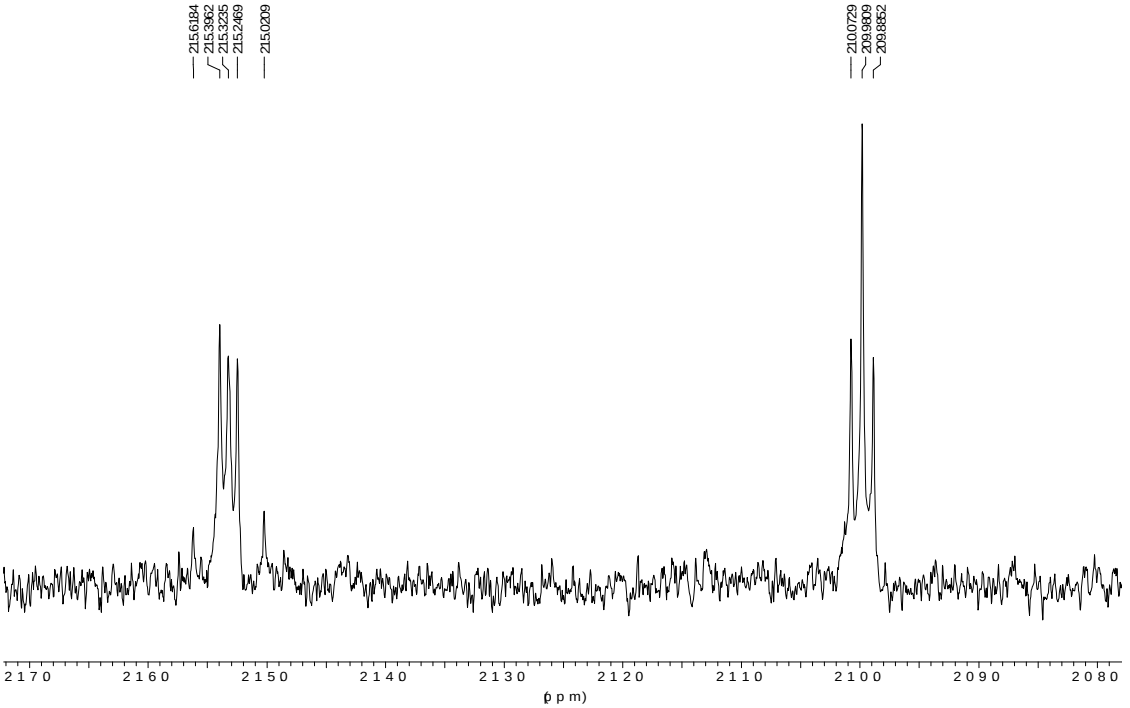

$^{13}C\{^{1}H\}$-RMN of **8** (carbonyl region)

Complex **9**

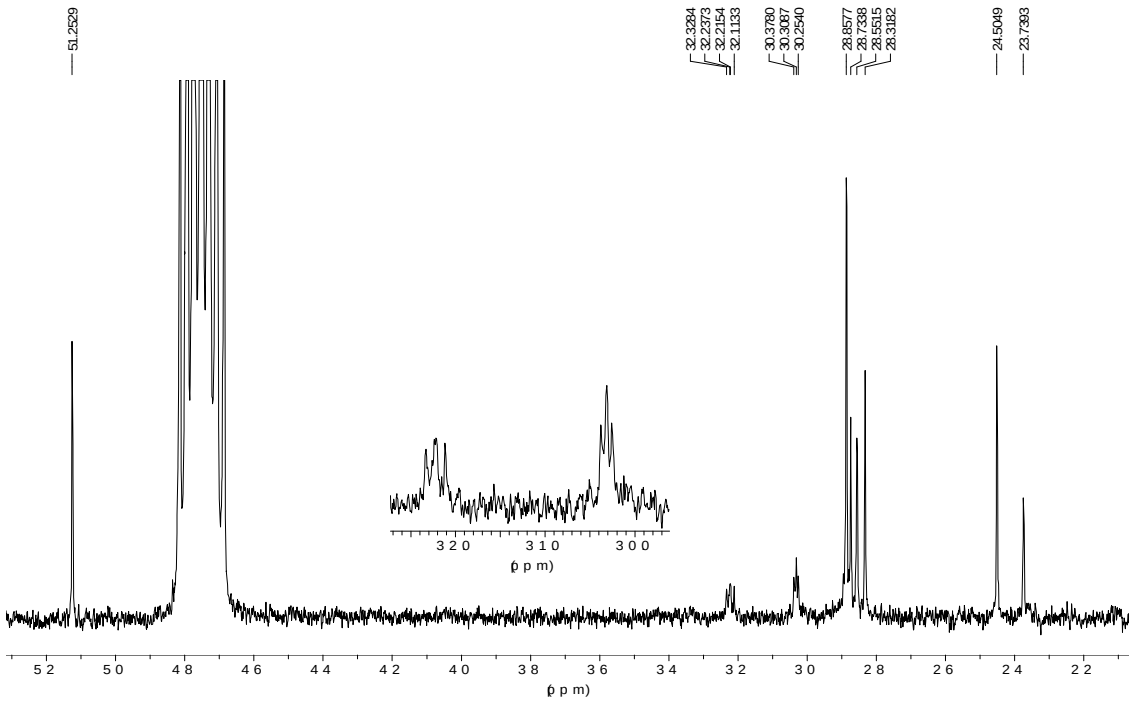

$^{13}C\{^{1}H\}$-RMN of **9** (aliphatic region)

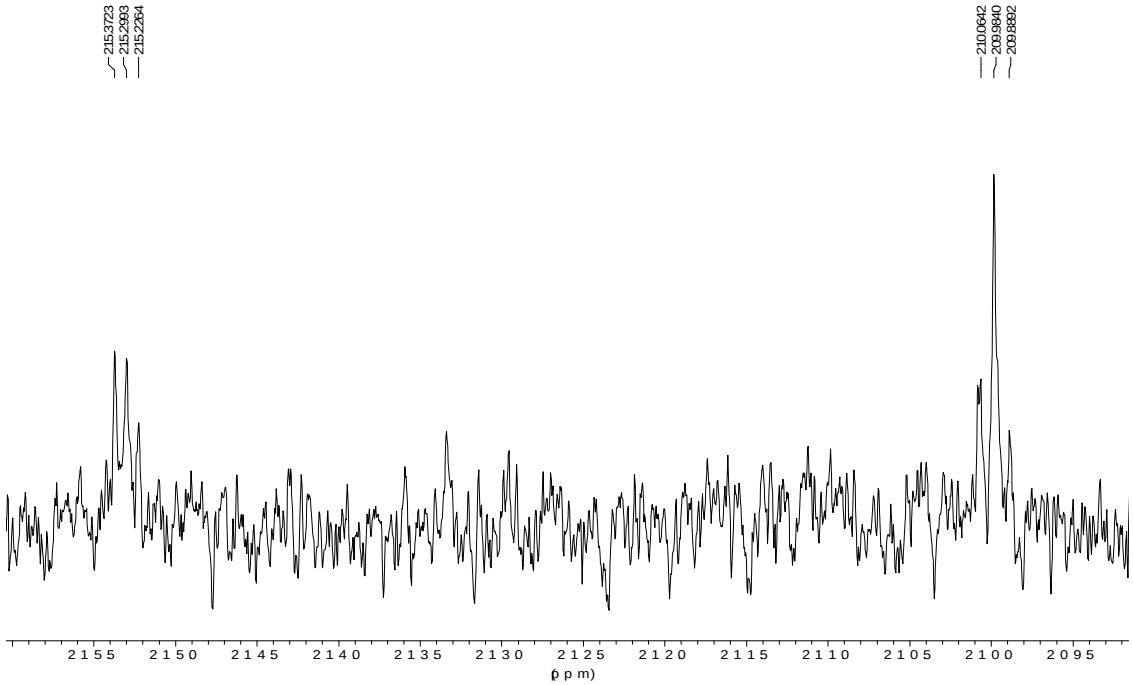

$^{13}C\{^{1}H\}$-RMN of **9** (carbonyl region)

Supporting Information 2

Compound	Γ / mol · cm^{-2}	A / $Å^2$
1	$(1.70 \pm 0.1) \times 10^{-10}$	99
2	$(1.64 \pm 0.03) \times 10^{-10}$	101
3	$(1.60 \pm 0.2) \times 10^{-10}$	100
4	$(1.75 \pm 0.04) \times 10^{-10}$	95
5	$(9.9 \pm 0.3) \times 10^{-11}$	167
6	$(8.9 \pm 0.8) \times 10^{-11}$	190
7	$(1.2 \pm 0.1) \times 10^{-10}$	140
8	$(8.7 \pm 0.3) \times 10^{-11}$	192
9	$(4.9 \pm 0.4) \times 10^{-11}$	340

Surface excess concentration (Γ) and estimated area occupied per molecule adsorbed in the water/air interface obtained from the surface tension measurements of water solutions of the compounds.

Supporting Information 3

	1	**4**	**7**
A_m (Å^2)	49±3	72±6	153±10
L_c (nm)	0.74±0.02	1.13±0.02	0.75±0.02
L_h (nm)	2.25±0.05	4.22±0.2	2.48±0.05
ρ_c (m^{-1})	8.32±0.05	7.60±0.05	7.55±0.05
ρ_h (m^{-1})	9.71±0.08	9.74±0.05	9.87±0.05
N_w	34±5	100±10	115±10
V_c (nm^3)	0.363±0.025	0.814±0.070	1.15±0.080
V_h (nm^3)	1.10±0.07	3.04±0.29	3.79±0.26
Scaling factor	0.959±0.005	1.007±0.002	1.004±0.001

Molecular parameters of the surfactants when forming macromolecular aggregates obtained from the fitted curves shown in Figure 8. A scaling factor multiplying the resulting hydrophilic electron density, as obtained from geometrical considerations, is necessary to correctly fit the absolute intensity scale (this factor has an effect on the intensity of 15% at most).

Supporting Information 4

An excluded volume routine was established using the following procedure:

First a search radius (typically in the 0.1 to 0.4 nm) is established. Random position spheres are produced in a cube which includes the molecule. Only the spheres at a distance larger than the summation of van der Waals radius plus search radius to any of the atoms are retained. Those spheres are generated in a high number, in such a way to define the excluded volume.

The excluded volume is calculated by generating random points in the cube and counting the proportion in the excluded volume as compared to the total volume.

The search radius is changed systematically to verify the independence of the excluded volume with the search radius. Little influence of search radius was obtained with the search radius.